Engineering Structures 229 (2021) 111612

Contents lists available at ScienceDirect

Engineering Structures

journal homepage: www.elsevier.com/locate/engstruct

Modeling recommendations for RC and CFST sections in LS-Dyna including bond slip

Mu-Zi Zhao [a,b,*], Dawn E. Lehman [c], Charles W. Roeder [c]

[a] Key Lab of Structures Dynamic Behaviour and Control (Harbin Institute of Technology), Ministry of Education, Heilongjiang, Harbin 150090, China
[b] School of Civil Engineering, Harbin Institute of Technology, Heilongjiang, Harbin 150090, China
[c] Dept. of Civil and Environmental Engineering, University of Washington, Seattle, WA 98195, USA

ARTICLE INFO

Keywords:
Concrete model
Bond-slip model
Finite element modeling
Cyclic response
Numerical simulation
Reinforced concrete
Composite construction

ABSTRACT

Modeling of reinforced concrete (RC) and concrete filled steel tube (CFST) sections is complex, because the model must be capable of capturing degradation of the concrete strength and stiffness in compression, confining effects, the response of the interface of the steel (either reinforcing bar or tube) and concrete. When RC and CFST are connected, (e.g., RC column-to-CFST pile connections or RC slab to CFST column connections), accurate and validated modeling is required for the steel tube, reinforcing steel, concrete fill, confined and unconfined concrete, bond between reinforcing bars and concrete, and bond between the tube and the concrete fill. To advance understanding and design of structural systems using RC and CFST components, a research study was undertaken to evaluate the accuracy various modeling approaches using LS-Dyna, which has a large library of concrete models and advanced modeling capabilities for bond. Large-scale experimental data was used to validate different modeling approaches for the RC and CFST components and their connections. Four concrete models were compared and evaluated using the test data; the new concrete damage plasticity model is found to provide the most accurate simulation of the cyclic behavior of concrete. The bond-slip behavior between steel and concrete was modelled using the cohesive material model. Model validation included comparison of the damage pattern and measured hysteresis curves. A summary of the recommended modeling parameters for use in future research and engineering practice is provided.

1. Introduction

The behavior of members and connections with concrete subjected to large displacements and/or cyclic loading is complex. Large-scale experimental studies have provided important information, understanding and data but the number of study parameters and specimen sizes are limited. In bridge construction, it is common to use RC piers as ductile, energy-dissipating components and CFST as piles and drilled shafts as the deep foundation elements. To accelerate construction, there is an interest in an economical, direct connection between these two elements. Similar connections are being explored for high-rise buildings. CFST components also are being considered for use as bridge piers [1,2] and columns in buildings.

To improve the understanding and design of these components, large-scale testing has been conducted [2–4]. These tests provide valuable insight into behavior and design of components and connections, but valid analytical models are needed to better understand behavior, conduct parametric studies to develop design equations and project specific applications; this includes accurate modeling approaches for the RC members, CFST members and their connections.

Prior research has used the general-purpose finite element (FE) program ABAQUS to predict the seismic behavior of RC [5,6] and CFST members [7,8]. These ABAQUS models commonly used the concrete damage plasticity model [9,10] to simulate the behavior of concrete. Although prior research has used this approach, this model cannot simulate the pinching behavior resulting from opening and closing of cracks [8], and can result in a large residual opening cracks on unloading [11]. To mitigate these issues, prior studies have introduced explicit, discrete interfaces to simulate cracking at specified locations, such as the base of column, where large cracks are expected to occur. This method can predict the experimental response but only if the crack locations are known [12]. As such, this is not a universally applicable approach.

There have been recent advancements in the concrete models in LS-

* Corresponding author at: School of Civil Engineering, Harbin Institute of Technology, Room 206, 73 Huanghe Road, Harbin 150090, China.
E-mail address: zhaomuzi@stu.hit.edu.cn (M.-Z. Zhao).

https://doi.org/10.1016/j.engstruct.2020.111612
Received 24 March 2020; Received in revised form 18 October 2020; Accepted 17 November 2020
Available online 13 December 2020

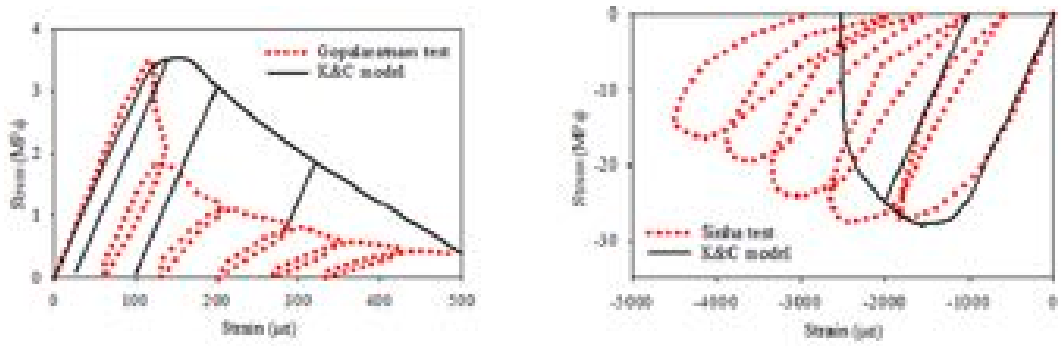

(a) K&C model

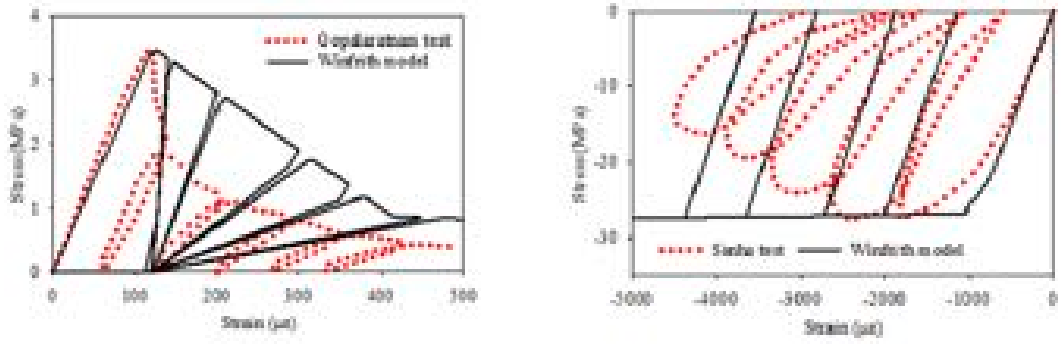

(b) Winfrith model

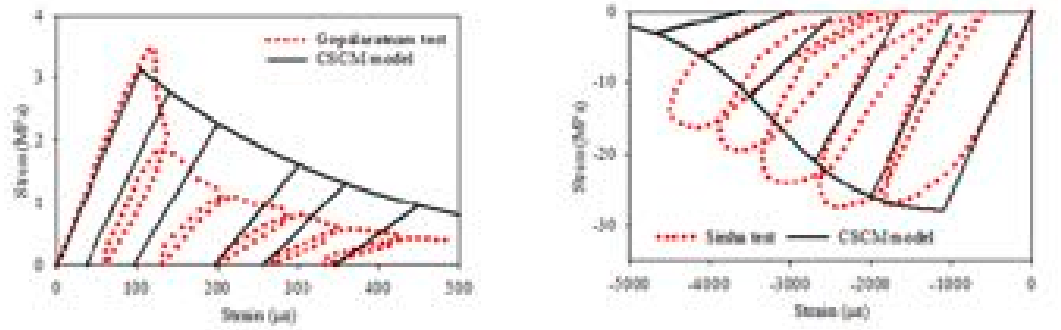

(c) CSC model

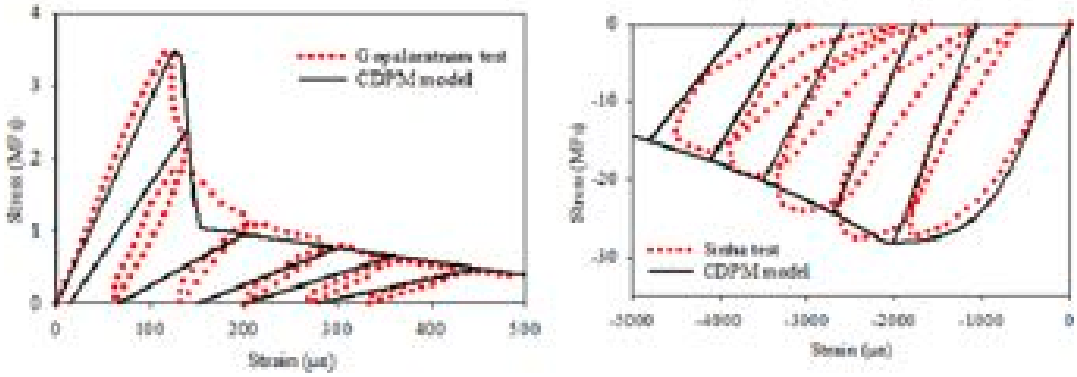

(d) CDP model

Fig. 1. Comparison of concrete cyclic behavior between test and predicted results using different concrete models.

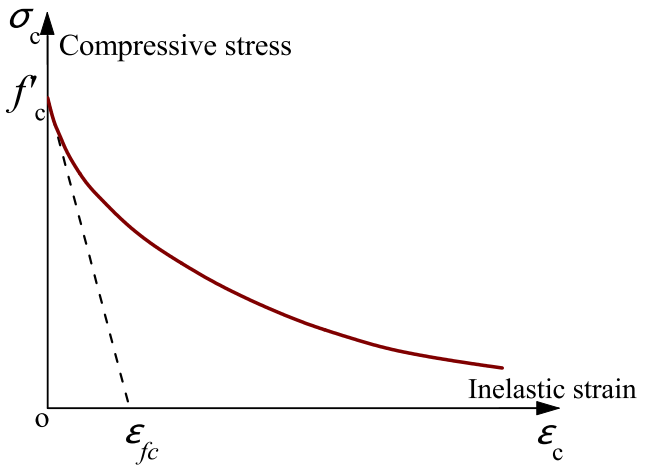

Fig. 2. Strain softening behavior of compression for CDP model.

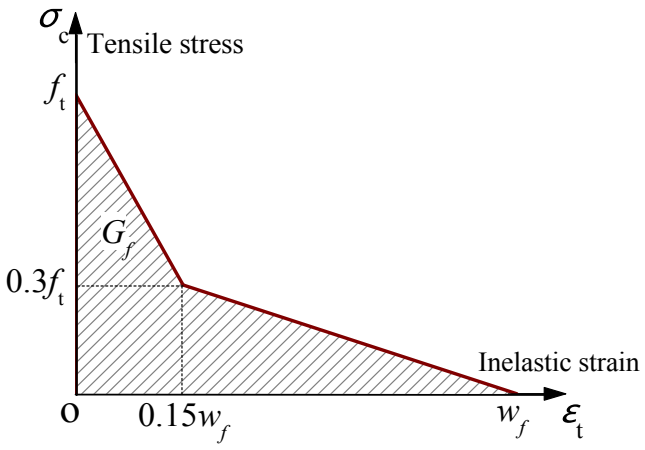

Fig. 3. Strain softening behavior of tension for CDP model.

Dyna. Recent work [13] indicated that the current Winfrith model (MAT085 in LS-Dyna) can simulate crack-induced pinching behavior. The concrete damage plasticity model (CDP model), denoted MAT273 in LS-Dyna [14,15], improves the prediction of the transition of tensile to compressive failure, which may occur for structural members under cyclic loading. Two other concrete models, the K&C model and CSC model, are also available in LS-Dyna with the capability to predict the mechanical behavior of concrete under complex stress states and had been evaluated [16,17] for simulation of the response of confined concrete. All four of these models were evaluated in this research.

Bond-slip behavior is critical to accurate simulation of RC, CFST and their connections. Reinforcing bars in RC is normally modeled by embedding bars into the concrete or steel bars sharing nodes with

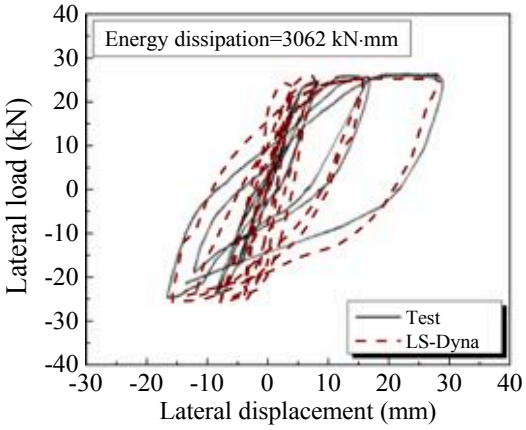

(a) Constant stress solid element (ELFORM=1)

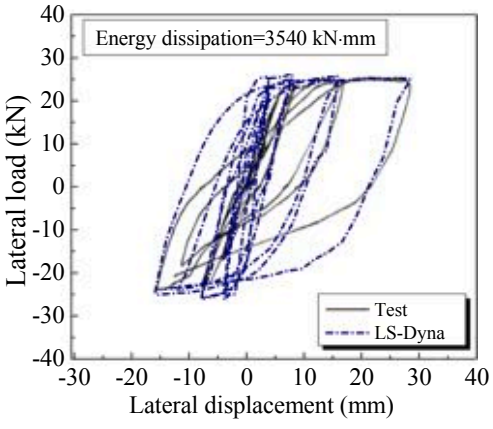

(b) Fully integrated S/R solid element (ELFORM=2)

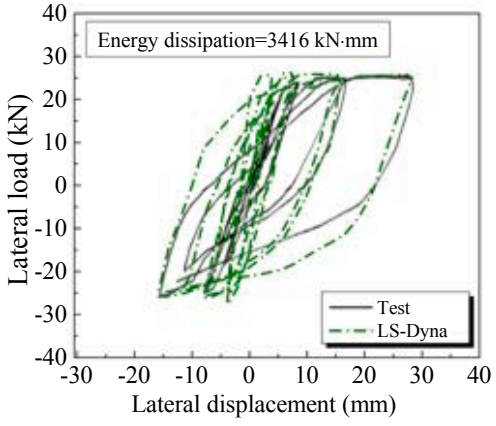

(c) Fully integrated S/R solid element for poor aspect ratio with efficient formulation (ELFORM=-1)

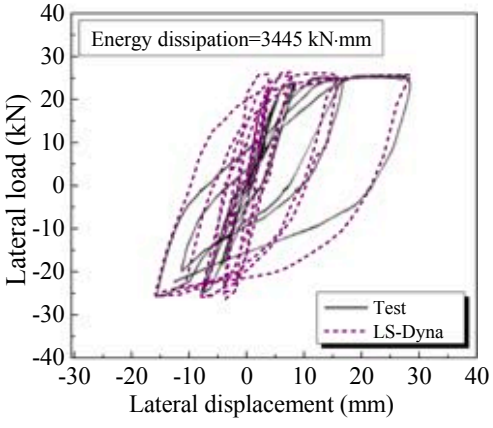

(d) Fully integrated S/R solid element for poor aspect ratio with accurate formulation (ELFORM=-2)

Fig. 4. Predicted load–displacement curve for RC column with different element type.

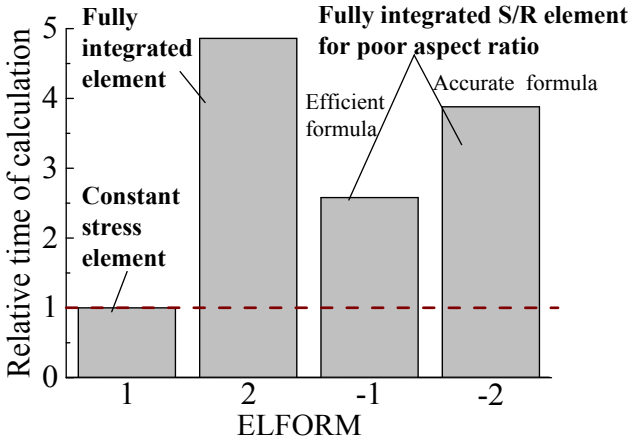

Fig. 5. Relative time of calculation versus element type.

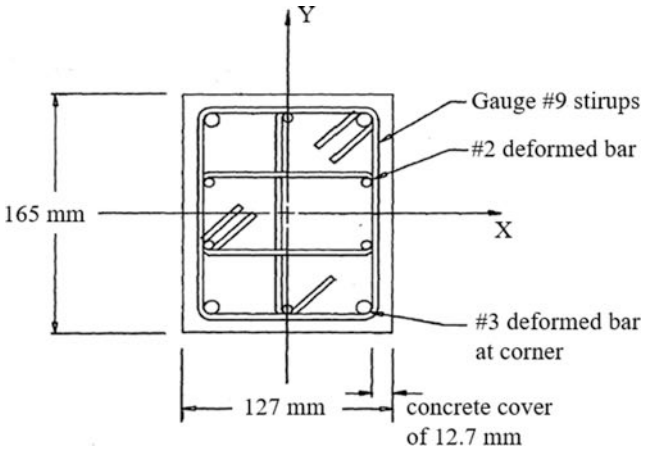

Fig. 7. Reinforcement configuration [33]

concrete elements, e.g., as used by Moon et al. [18,19], and Wang et al. [20]. This simulates perfect bond between reinforcement and concrete and ignores bond-slip. However, with perfect bond, the predicted results tend to leading to less pinched hysteretic curves and reduced deformation [11]. Researchers have proposed bond-slip models for reinforcement-concrete interface, and one of the earliest studies modelled monotonic bond behavior of reinforcing bar in RC [21]. This model was characterized by its yield function and flow rule which consider the effect of normal stress as well as the shear dilation caused by ribs of reinforcing bar. Another interface model for FE analysis was simulated the cyclic behavior of bar-concrete interface with an iterative algorithm based on monotonic and cyclic pull-out tests [22,23]. Other researchers [24,25] developed bond-slip models to account for the influence of damage in the surrounding concrete. A bond-slip model that provides simple expressions to reasonably predict the monotonic and cyclic behavior of bar-concrete interface have also been developed [11,26], and damage of concrete, cross-section contraction of reinforcing bar and cyclic deterioration of bond were all considered. This paper adopted this model due to its easy application and comprehensive approach [11,26].

Bond slip between the steel tube and concrete fill of CFST has been studied [e.g.,18,27–29], and this behavior is normally modeled as Coulomb friction:

$$F_f \leqslant \mu F_n \tag{1}$$

where F_f is the interface force, F_n is the force normal to the interface and μ is the coefficient of friction, which has been between 0.3 and 0.6 [18,30–32]. However, bond-slip behavior in CFST members is not always accurately predicted using this method. Spiral-weld tubes develop mechanical bond at the welds and all tubes develop binding action that can increase the bond between concrete core and steel tube. As such, a more accurate approach to model the bond-slip behavior in CFST is needed to model these tubes.

This paper uses the commercially available LS-Dyna nonlinear

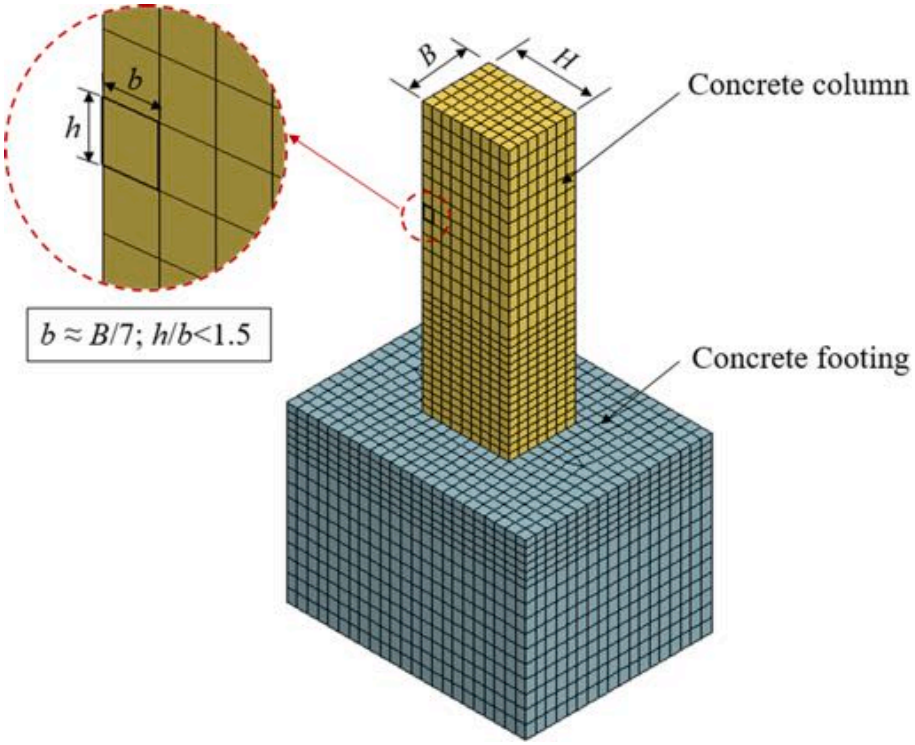

Fig. 6. Model of RC Column Tests: Concrete Elements.

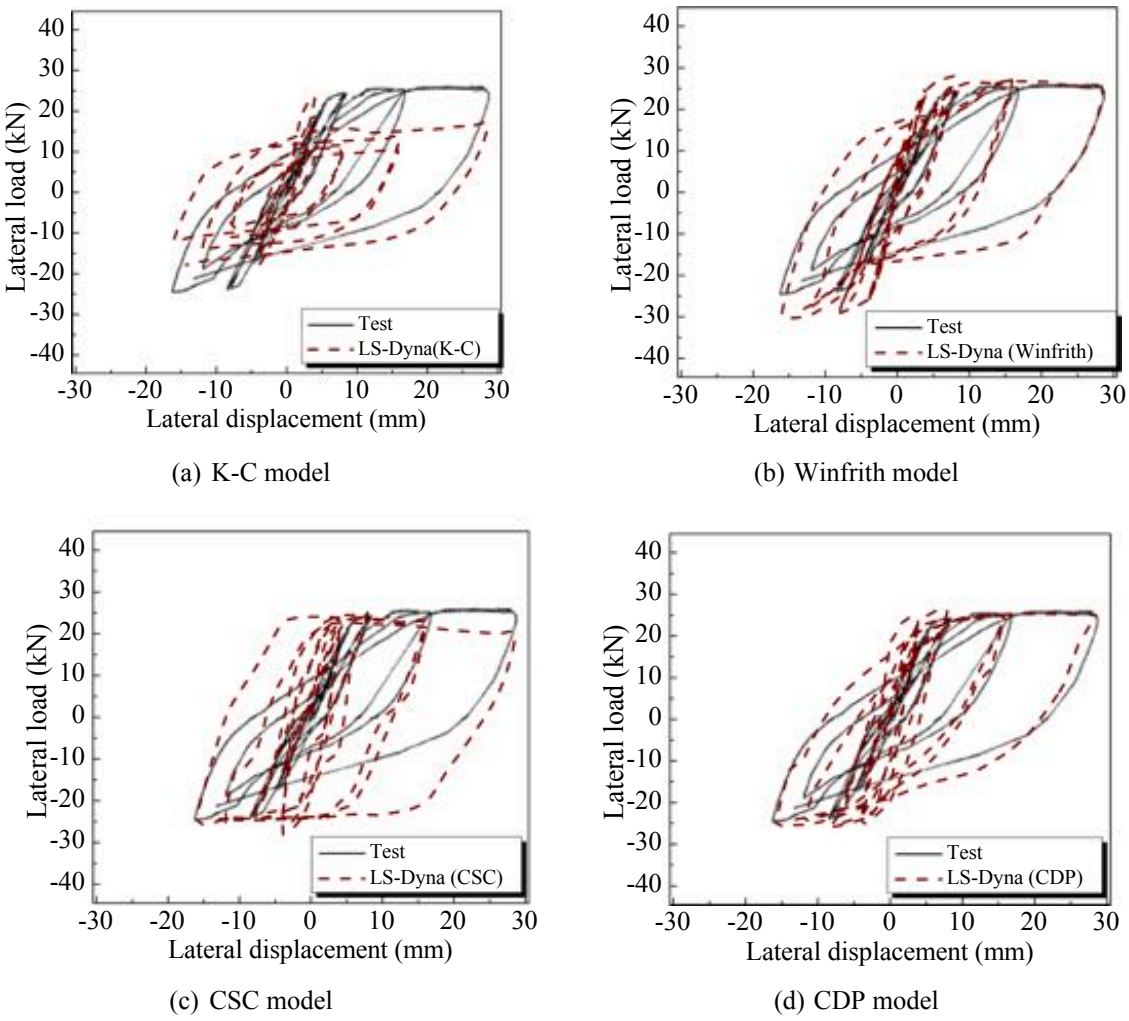

Fig. 8. Predicted load–displacement curve for RC column with various concrete model.

analysis program to overcome the challenges observed in prior studies and develop modeling recommendations to accurately simulate the seismic behavior of RC and CFST members and connections. The research used a set of large-scale, well-vetted experiments to determine the modeling parameters for each type of component: RC column tests [33], CFST component and connection tests [3] and CFST to RC direct connection tests [4]. A different set of experiments is used for validation. For each type of component, the modeling approach was developed as follows. First, the four previously discussed concrete models were initially evaluated. Next, the element type for the concrete was evaluated, including consideration of the mesh size and element aspect ratio. Using these results, a full model was developed including appropriate bond-slip models to simulate the interface between the concrete and steel. The values for the modeling parameters were determined by comparing predictions to the experimental results. Finally, the proposed modeling approach was verified using other test data, RC column tests [34] and embedded column base connection for CFST [35]. The comparison included force–displacement response data, observed yielding, concrete damage. A summary table of the recommended modeling parameters and element types is provided.

This paper results in qualitative and quantitative results to evaluate the accuracy of different modeling approaches for both RC and CFST section using the advanced capabilities of LS-Dyna. The information provided in this paper is expected to provide other researchers and practicing engineers validated modeling approaches for RC and CFST components and their connections. It is noted that although many researchers and practicing engineers use advanced nonlinear modeling methods, there are few papers that provide modeling recommendations based on a methodical approach to evaluating available methods. These results will both provide a starting point for others utilizing the capabilities of LS-Dyna, but has also provided the basis for the research team has to investigate new strength design equations and new connections between RC and CFST components.

Table 1
Deviation of predictions with different concrete models for RC column.

Tests	K-C		Winfrith		CSC		CDP	
	V_s/V_m [a]	G_s/G_m [b]	V_s/V_m	G_s/G_m	V_s/V_m	G_s/G_m	V_s/V_m	G_s/G_m
RC column [33]	0.9	1.3	1.1	1.6	1.0	2.1	1.0	1.6

Note: [a] the V_s/V_m is the simulated-to-measured strength ratio.
[b] the G_s/G_m is the simulated-to-measured energy dissipation ratio.

2. Modeling parameters

2.1. Concrete constitutive model

LS-Dyna has a suite of constitutive models to simulate the mechanical behavior of concrete. The four concrete constitutive models that are most commonly used are as follows [20,36,37] (material designations used in LS-Dyna are given in parentheses): the K&C model (MAT072R3),

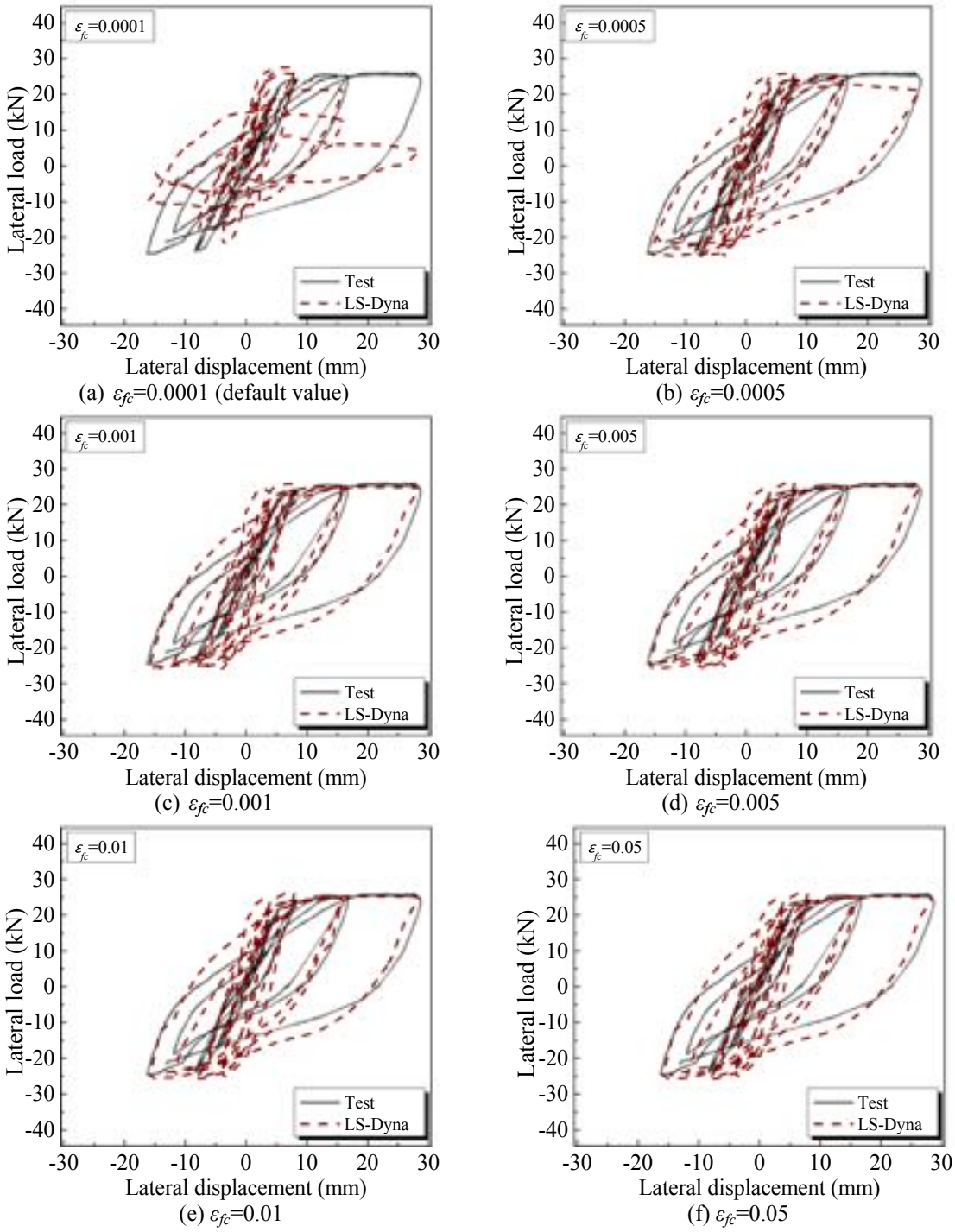

Fig. 9. Predicted load–displacement curve for RC column with different damage parameters of concrete.

the Winfrith model (MAT085), the CSC model (MAT159) and the concrete damage plasticity model or CDP model (MAT273). The predictions of these four concrete models were compared to the experimentally-derived cyclic curves of axially loaded, unconfined plain concrete specimens in both tension and compression [38–40] (Fig. 1). In the figure, positive stress indicates tension, and negative stress indicates compression.

2.1.1. K&C Concrete model

The K&C model ("MAT_CONCRETE_DAMAGE_RELIII" in LS-Dyna) [41] uses simple functions to characterize three independent failure surfaces (i.e., the yield, the maximum and the residual strength surfaces), which are each expressed using Eq. (2):

$$F_i(p) = a_{0i} + \frac{p}{a_{1i} + a_{2i}p} \tag{2}$$

where i donates the failure surface and a_{0i}, a_{1i} and a_{2i} are parameters calibrated for each failure surface from experimental data.

Beyond the yield-strength surface, the current failure surface is linearly interpolated between the yield strength surface and maximum strength surface, expressed by Eq. (3):

$$F_i(I_1, J_2, J_3) = r(J_3)[\eta(\lambda)(F_m(p) - F_y(p)) + F_y(p)] \tag{3}$$

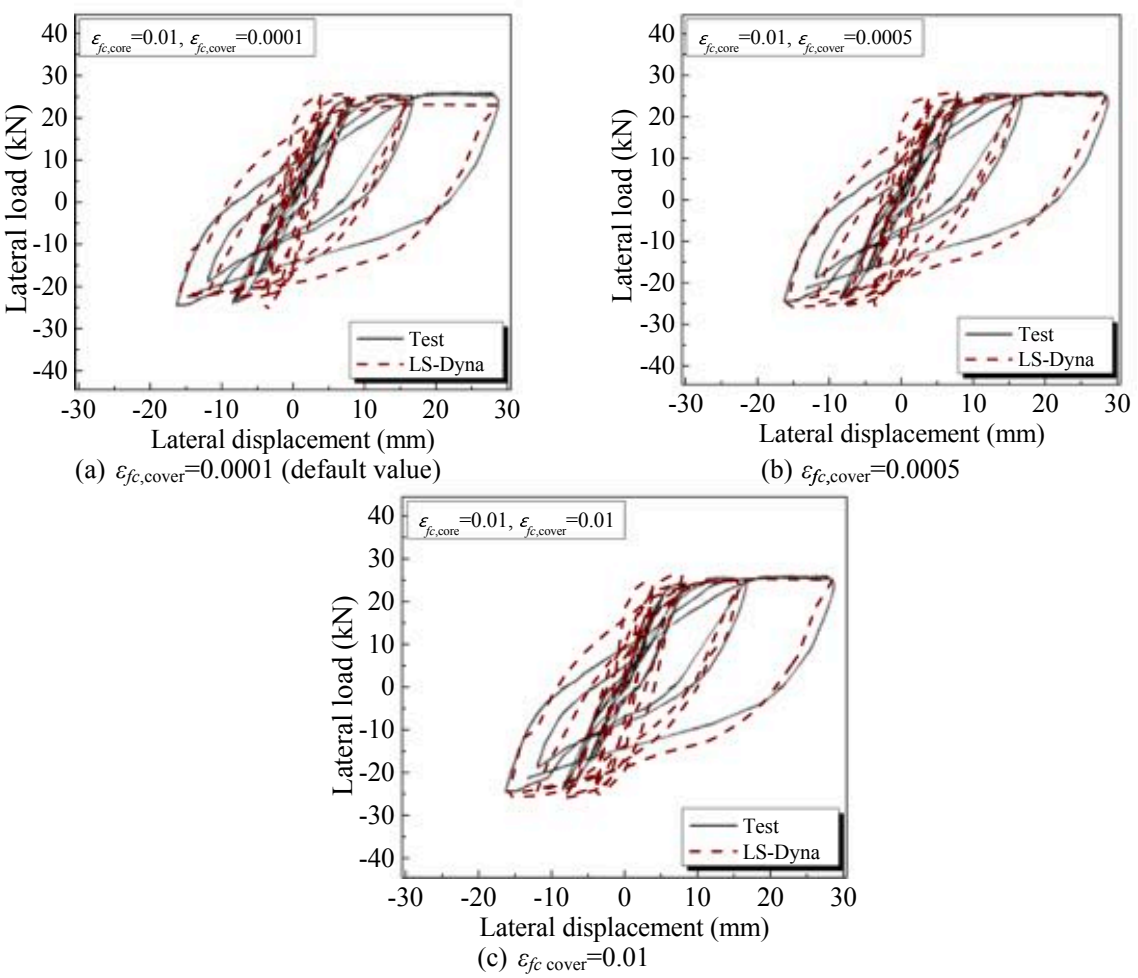

Fig. 10. Predicted load–displacement curve for RC column with different damage parameters of concrete cover.

where I_1 is the first invariant of stress tensor; J_2 and J_3 are the second and third invariant of deviatoric stress tensor, respectively; the term r (J_3) is the scale factor in the form of William-Warnke equation [42]; the term λ is the modified effective plastic strain, which is between 0 and λ_m in Eq. (3); the term η is a function of λ with $\eta(0) = 0$ and $\eta(\lambda_m) = 1$. The λ_m and the relationship between η and λ is required to be input by users.

The current failure surface after reaching the maximum strength surface is also determined as Eq. (3), while the λ is between λ_m and λ_{max}. The η is equivalent to zero when $\lambda > \lambda_{max}$.

The K&C concrete model requires a_{0i}, a_{1i} and a_{2i} parameters and a series of λ and η values to simulate the hardening and softening behavior of concrete. However, these parameters are auto-generated in LS-Dyna based solely on the unconfined compression strength of concrete (f'_c). In this context, as recommended by the LS-Dyna User Manual-Volume II [43], the maximum shear failure surface parameter A0 (a_{0m} in the Eq. (2)) is taken as $-f'_c$ and the rest variables are kept as default values.

Fig. 1a shows that the K&C model tends to overestimate the degradation of concrete compressive strength and underestimate the strength degradation in tension, and the stiffness reduction in both directions is not observed in the simulation. Accordingly, K&C concrete model may not be appropriate to estimate the cyclic behavior of concrete.

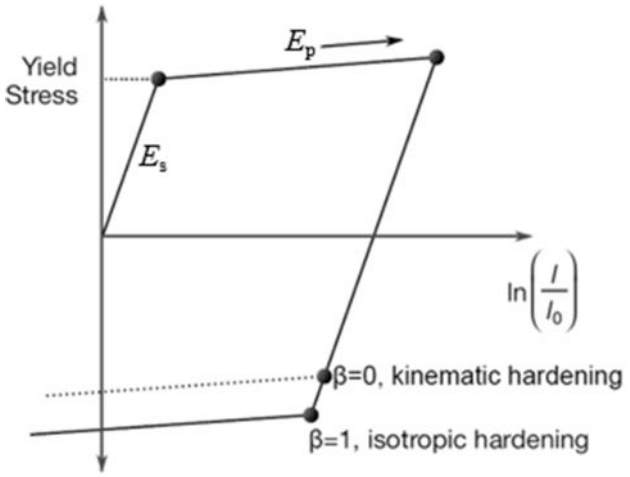

Fig. 11. Elastic-plastic behavior with kinematic and isotropic hardening [43]

2.1.2. Winfrith model

The Winfrith model ("MAT_WINFRITH_CONCRETE" in LS-Dyna) is based on a smeared-crack model [44]. This model assumes an elastic-perfectly plastic behavior in compression and its yield surface is developed based on the four-parameter plastic surface [45] presented in Eqs. (4) and (5).

$$F_i(I_1, J_2, cos3\theta) = a\frac{J_2}{(f'_c)^2} + \lambda\frac{J_2}{f'_c} + b\frac{I_1}{f'_c} - 1 \quad (4)$$

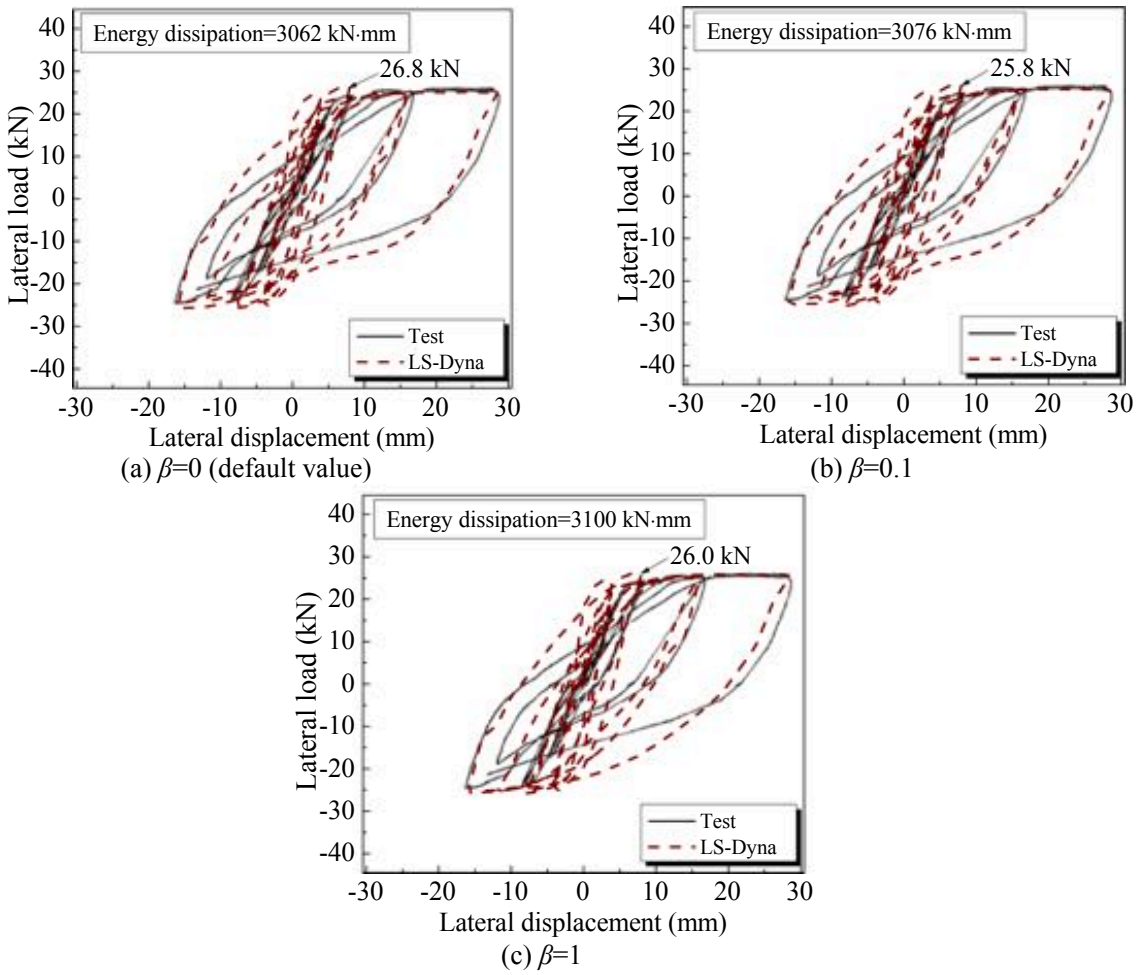

Fig. 12. Predictions of RC column with hardening parameters of 0 and 1.

$$\lambda = \begin{cases} k_1 cos[\frac{1}{3} cos^{-1}(k_2 cos3\theta)] \ (cos3\theta \geqslant 0) \\ k_1 cos[\frac{\pi}{3} - \frac{1}{3} cos^{-1}(-k_2 cos3\theta)] \ (cos3\theta < 0) \end{cases} \quad (5)$$

where θ is Lode angle; a, b, k_1, k_2 are parameters which are a function of (f_t/ f'_c), which can be auto-generated in LS-Dyna; the variable f_t donates the tensile strength of concrete.

In the Winfrith model, the post-cracked behavior of concrete under tension can be defined by (1) linear strain softening without strain-rate effect or (2) bilinear strain softening including strain-rate effects. The linear strain softening option was selected for the simulation because the experiments used in this paper were quasi-static; strain-rate effects are ignored. The crack width, w, at which the normal tensile stress is zero, is given by:

$$w = \frac{2G_f}{f_t} \quad (6)$$

where G_f is the fracture energy which can be determined as Eq. (7) [46]

$$G_f = 73 f_c^{'0.18} \quad (7)$$

where the f'_c is the uniaxial cylinder concrete compressive strength in MPa.

Fig. 1b shows no degradation of concrete strength in compression and the decrease of tensile strength is significantly smaller than that in the experiment. Therefore, the Winfrith concrete model cannot reasonably estimate the performances of concrete under cyclic loading.

2.1.3. CSC model

The CSC model was developed for LS-Dyna by the U.S. Department of Transportation [16] and is a continuous surface-cap model which combines the shear failure surface with a hardening compaction surface. The yield function is developed based on three invariants (i.e., I_1, J_2 and J_3) and ca-hardening parameter, κ:

$$f(I_1, J_2, J_3) = J_2 - \Re(J_3)^2 F_f^2(I_1) F_c(I_1, \kappa) \quad (8)$$

In the equation, F_f is the shear failure surface, as given by Eq (10); (J_3) is the invariant reduction factor [47]; and $F_c(I_1, \kappa)$ is the hardening cap, as given by Eqs. (9)–(12).

$$F_f(I_1) = \alpha - \lambda exp^{-\beta I_1} + \gamma I_1 \quad (9)$$

In Eq. (9), α, λ, β, γ are parameters determined by fitting the model surface to strength measurement from triaxial compression tests.

$$F_c(I_1, \kappa) = \begin{cases} 1 - \frac{(I_1 - L(\kappa))^2}{(X(\kappa) - L(\kappa))^2} \ I_1 \geqslant L(\kappa) \\ 1 \ I_1 < L(\kappa) \end{cases} \quad (10)$$

$$L(\kappa) = \begin{cases} \kappa \ \kappa \geqslant \kappa_0 \\ \kappa_0 \ \kappa < \kappa_0 \end{cases} \quad (11)$$

$$X(\kappa) = L(\kappa) + R F_f(I_1) \quad (12)$$

where the R is the input parameter; and κ_0 is the value of J_1 at the initial intersection of the cap and shear surfaces before hardening is engaged (before the cap surface expands or shrinks). After reaching the

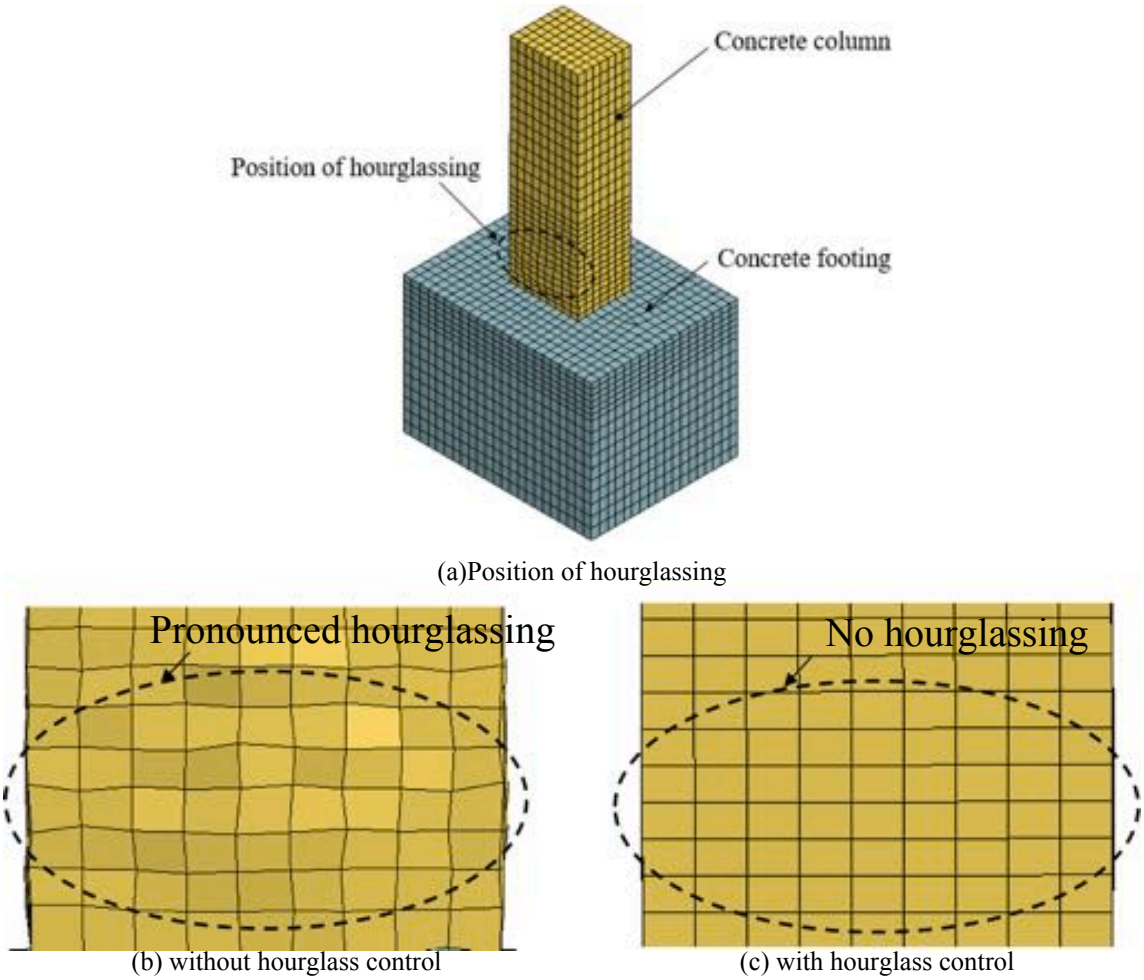

Fig. 13. Hourglass pattern in the bottom of RC column.

yield surface, the cap adjusts to simulate plastic volume change. The cap extends (e.g., $X(\kappa)$ and κ increase) to simulate plastic volume compaction; while the cap shrinks ($X(\kappa)$ and κ decrease) as the plastic volume expansion occurs. The adjustment of cap is based on the hardening rule given in Eq. (13).

$$\varepsilon_v^p = W(1 - exp^{-D_1(X-X_0)-D_2(X-X_0)^2}) \tag{13}$$

where the ε_V^p is the plastic volume strain, W donates the maximum plastic volume strain, D_1 and D_2 are parameters, and X_0 is the initial location of cap surface for $\kappa = \kappa_0$.

The parameters in Eqs. (12) and (13) (i.e., X_0, W, D_1, D_2 and R) are determined by fitting to the pressure-volumetric strain curves in hydrostatic compression and uniaxial strain experiment.

The damage formation in CSC model is presented as Eq. (14).

$$\sigma_{ij}^d = (1 - d)\sigma_{ij}^{vp} \tag{14}$$

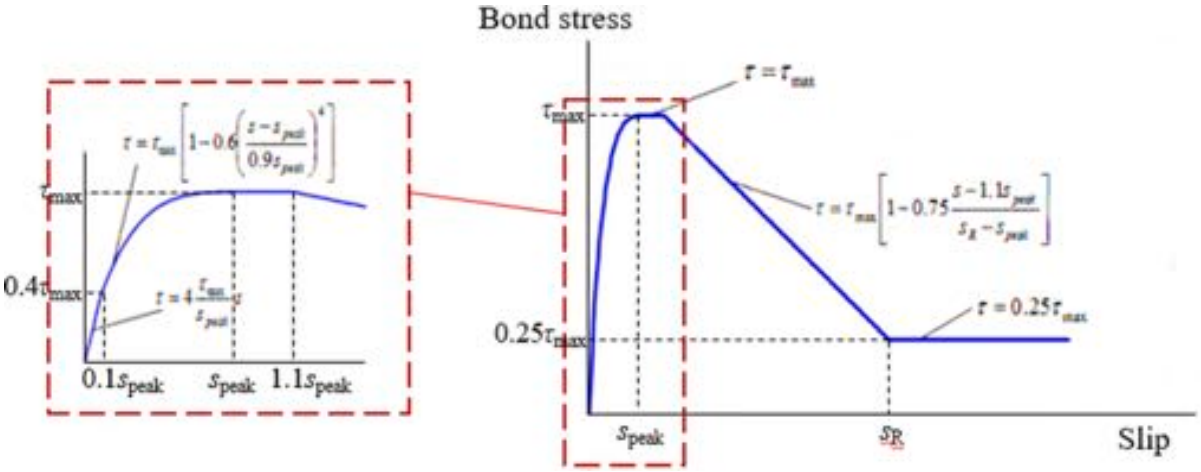

Fig. 14. Bond-slip behavior proposed by Murcia-Delso et al. [26]

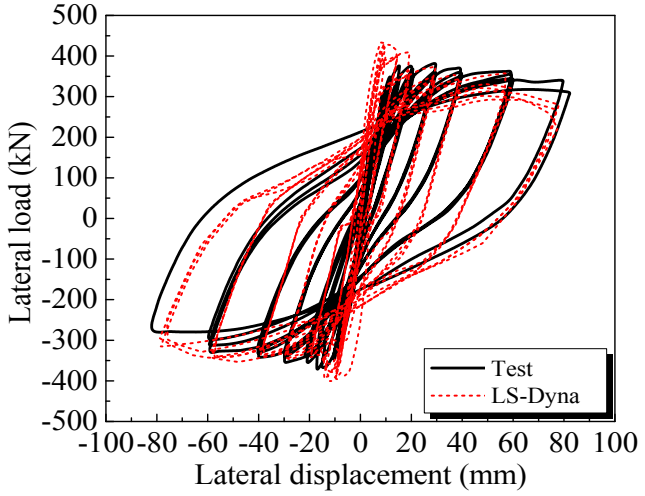

Fig. 15. Comparison between the predicted and test results from Xiao's experiment.

In the expression, σ_{ij}^{d} and σ_{ij}^{vp} are stress tensors with and without consideration of damage, respectively, and d is a scalar damage parameter. The value of d increases from zero (undamaged) to one (fully damaged) and accumulates with brittle and ductile damage threshold, τ_b and τ_d. Brittle damage accumulates only when the pressure is tensile and depends on maximum principle strain, ε_{max}:

$$\tau_b = \sqrt{E\varepsilon_{max}^2} \tag{15}$$

Ductile damage accumulates only when the stress is compressive and depends on the total strain components, ε_{ij}:

$$\tau_d = \sqrt{\frac{1}{2}\sigma_{ij}\varepsilon_{ij}} \tag{16}$$

In this context, the damage accumulation during strain softening can be calculated as:

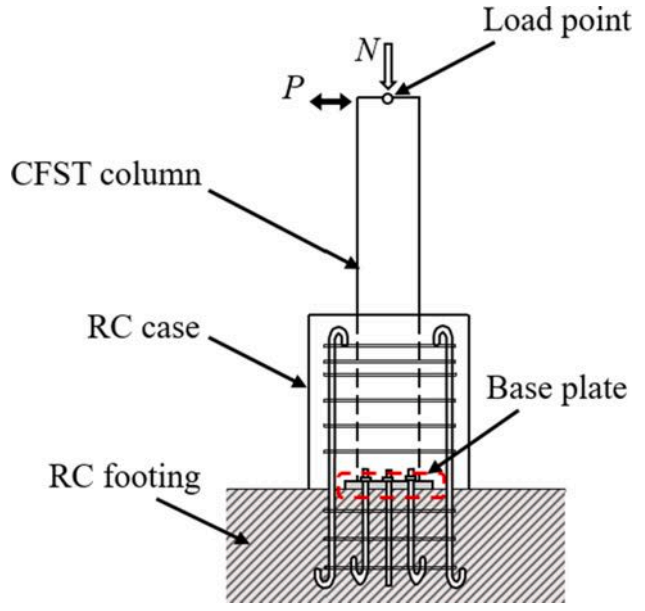

Fig. 16. Schematic of concrete-encased column base specimen [4].

$$d(\tau) = \begin{cases} \dfrac{0.999}{D}\left(\dfrac{1+D}{1+Dexp(-C(\tau - r_{0b}))} - 1\right) \text{ for brittle damage } \tau = \tau_b \\ \dfrac{D_{max}}{B}\left(\dfrac{1+B}{1+Bexp(-A(\tau - r_{0d}))} - 1\right) \text{ for ductile damage } \tau = \tau_d \end{cases} \tag{17}$$

The default values of the above parameters, which describe the material properties of normal strength concrete [43], are used in LS-Dyna as shown in Fig. 1c. The CSC model slightly overestimates the compressive strength degradation and the predicted fracture energy in tension is somewhat higher than that in the test. The modest difference between prediction and test results indicates that this model may be acceptable for evaluation of the cyclic behavior of concrete.

2.1.4. CDP model

The concrete damage plasticity model (CDP model, MAT273 in LS-DYNA) [14,15] characterizes the failure process of concrete under multi-axial loading. The yield function given by Eq. (18) depends on the volumetric effective stress (σ_v), the norm of deviatoric effective stress (ρ), Lode angle (θ) and the hardening variable (k_p). The details of flow rules and hardening laws are presented elsewhere [15].

$$\begin{aligned} f_p = (\sigma_v, \rho, \theta, \kappa_p) = \{[1 - q_1(\kappa_p)]\left(\frac{\rho}{\sqrt{6}f_c'} + \frac{\sigma_v}{f_c'}\right)^2 + \sqrt{\frac{3}{2}}\frac{\rho}{f_c'}\}^2 \\ + m_0 q_1 \kappa_{p_{q2}}(\kappa_p)\left[\frac{\rho}{\sqrt{6}f_c'} r(cos\theta) + \frac{\sigma_v}{f_c'}\right] - q_1\left(\kappa_{p_{q2}}\right)^{\kappa_p} \end{aligned} \tag{18}$$

In the expression, m_0 is the friction parameter given by Eq. (19), r (cosθ) is the function controlling the shape of the deviatoric section given by Eq. (20).

$$m_0 = \frac{3\left(f_c'^2 - f_t^2\right)}{f_c' f_t}\frac{e}{e+1} \tag{19}$$

$$r(cos\theta) = \frac{4(1-e^2)cos^2\theta + (2e-1)^2}{2(1-e)^2 cos\theta + (2e-1)\sqrt{4(1-e^2)cos^2\theta + 5e^2 - 4e}} \tag{20}$$

and e is the eccentricity parameter, which can be calculated by Eq. (21) [43].

$$e = \frac{f_t\left(f_{bc}^2 - f_t^2\right)}{f_{bc}\left(f_c'^2 - f_t^2\right)} \tag{21}$$

In the expression, f_{bc} is the biaxial compressive strength of concrete, which is equal to $1.16f'_c$. The damage function in CDP model is:

$$\sigma = (1 - w_t)\sigma_t + (1 - w_c)\sigma_c \tag{22}$$

where σ is the effective stress tensor, σ_c and σ_t are the positive and negative parts of the effective stress, w_t and w_c are tensile and compressive damage parameters varying from 0 (undamaged) to 1 (fully damaged). The compressive damage is described by the exponential stress-inelastic displacement law as illustrated in Fig. 2, and ε_{fc} controls the strain softening behavior and is the intersection between the tangential line of the compressive strain softening curve and the x-axis.

There are three forms of the tensile damage model in the CDP model: linear, bilinear and exponential. The bilinear damage model illustrated in Fig. 3 was used for this study due to its reasonable estimation of experimental data [15]. In the figure, G_f is the fracture energy represented by the shadowed area under the strain softening curve; and w_f is the maximum tensile inelastic strain, which can be estimated as $w_f = 4.444G_f/f_t$ [15].

The default value of ε_{fc} (0.0001) was used in the comparison of Fig. 1d, and the CDP model shows good agreement with the test results and provides the best prediction of the four concrete models. Accordingly, the CDP model can be used to evaluate cyclic loading of concrete.

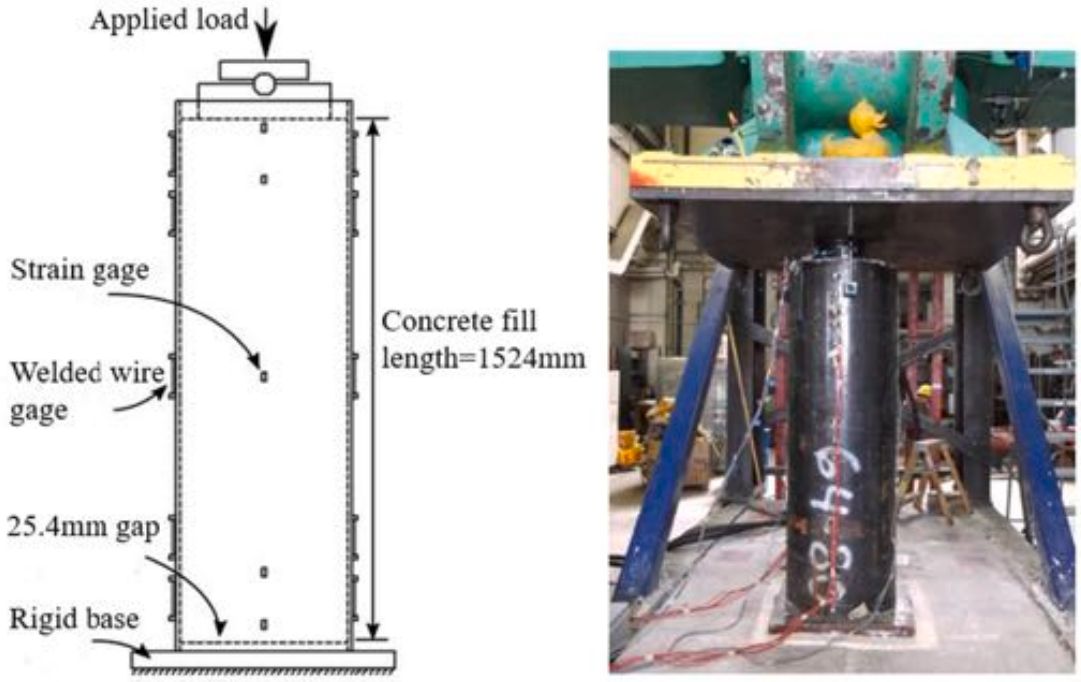

(a) Test aparatus

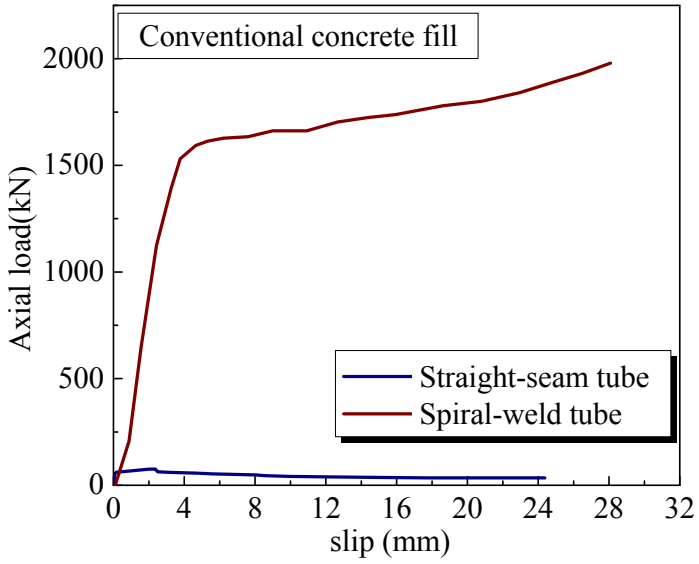

(b) Measured responses

Fig. 17. CFST Bond Tests [3].

2.2. Selection of concrete element and mesh size

For the modeling, 8-node reduced integrated solid element was used to simulate the concrete behavior. There are 4 commonly-used solid element types in LS-Dyna: the constant stress solid element (ELFORM = 1), fully integrated S/R solid element (ELFORM = 2), and fully integrated S/R solid element for poor aspect ratio with efficient and accurate formulations, respectively (ELFORM = −1 and −2). The predictions for these 4 element types are compared with the RC column experimental data [33] in Fig. 4. The comparison shows that all of the models predicted specimen resistance with acceptable accuracy, but the constant stress solid element provided the best estimation of the hysteretic behavior of the test specimen. Further, Fig. 5 shows that constant stress solid element provided the best relative calculation time of the four models. The calculation time for the simulation with fully integrated S/R solid element was at least 2.6 times the calculation with constant stress solid element. This element has both accuracy and computational efficiency. Therefore, the constant stress solid element was used in this study.

The mesh size depends on the dimension and shape of specimen, but computation time will be large if the mesh is too fine, while an excessively large mesh would adversely affect the accuracy of the prediction.

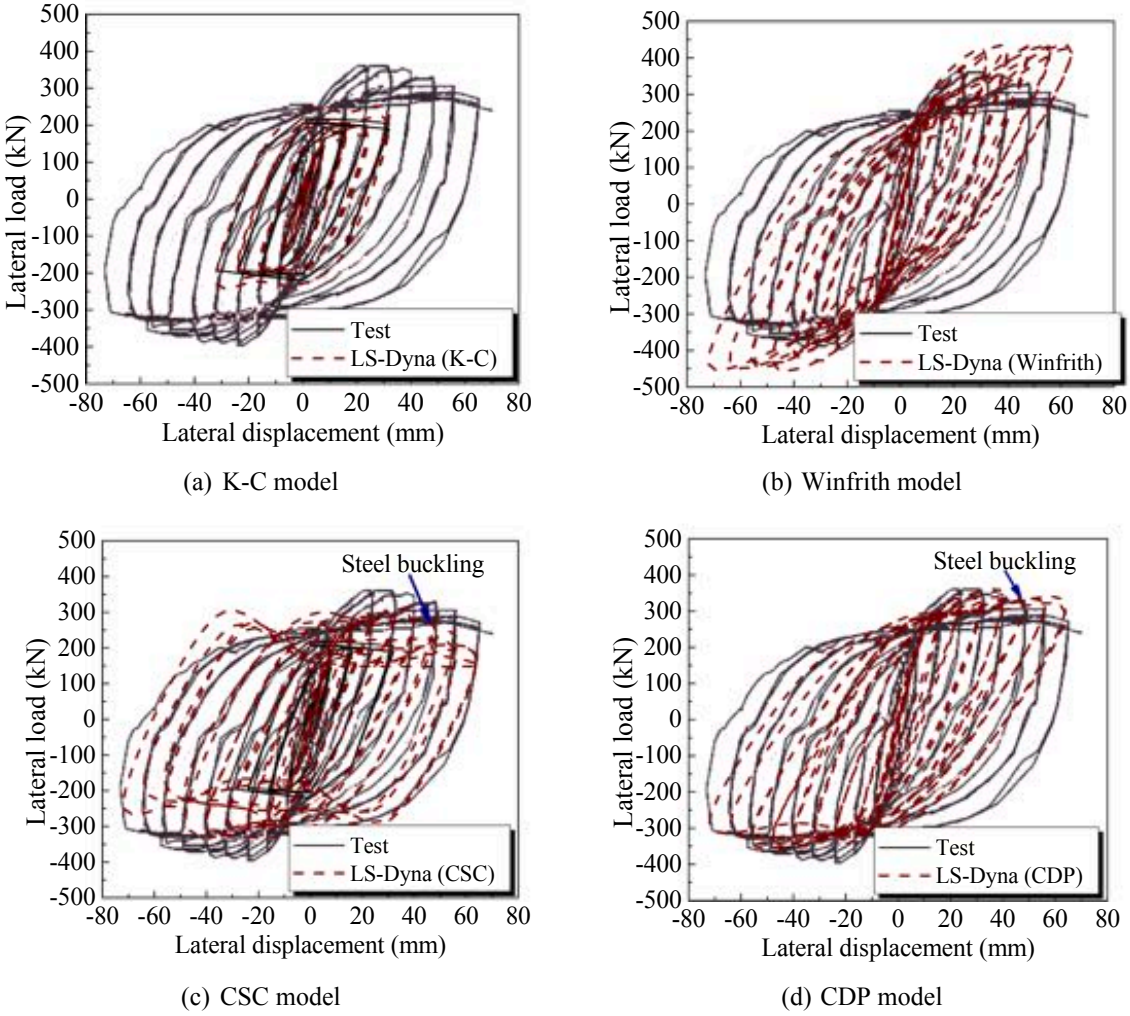

Fig. 18. Predicted load–displacement curve with various concrete model.

On average, the mesh size used in this study is $B/7$ where B is the length of short side in concrete column (see Fig. 6) and the concrete sections in the regions of expected nonlinear action in the steel were more densely meshed to accurately simulate the stress states and crack patterns of concrete. With this approach, the calculation time can be less than 3 hours using the supercomputer Stampede2 in Texas Advanced Computing Center. The prediction with a mesh size of $B/14$ had a very small difference (0.4%) in predicted results from the $B/7$ mesh size. Further, the aspect ratio (h/b) of each element was less than 1.5 to minimize its influences on the predicted results.

3. Model development for RC components

3.1. Experimental specimen for model Development: RC column test [33]

Low and Moehle [33] tested five rectangular column specimens with dimensions of 127 × 165 × 514.4 mm subjected to uni- and bi-directional, cyclic loading. The loading history and direction were the study parameters. Specimen I, which was subjected to uniaxial loading about the weak axis, was analyzed (shown in Fig. 4). The specimen reinforcement is shown in Fig. 7. The yield strengths of No. 3 and No. 2 reinforcing bars were 448 MPa and 444 MPa, respectively. The transversal rebar was No. 9 wire with the yield strength of 414 MPa. The specimen had a concrete uniaxial compressive strength of 35.6 MPa. A constant axial load of 44.5 kN was applied to column.

Table 2
Deviation of predictions with different concrete models for CFST column.

Tests	K-C		Winfrith		CSC		CDP	
	V_s/V_m	G_s/G_m	V_s/V_m	G_s/G_m	V_s/V_m	G_s/G_m	V_s/V_m	G_s/G_m
CFST column [4]	0.7	0.1	1.2	0.5	0.8	0.6	1.0	0.6

3.2. Analytical model

Both the CSC and CDP models predict the behavior of unconfined concrete under cyclic loading with acceptable accuracy. However, most of the concrete in ductile RC columns is confined by transverse reinforcement. As such, the accuracy of the predictions using the four concrete models for confined concrete in RC column under cyclic loadings was of critical importance. The predictions using different concrete models and comparing with the experimental results are shown in Fig. 8. The K-C model does not provide a reasonable prediction of the cyclic behavior of RC column, because the predicted initial stiffness and degradation of ultimate strength were notably higher than test results. The Winfrith model accurately predicted the resistance but did not capture deterioration in concrete strength, which is a critical aspect to be simulated in nonlinear analysis of concrete components, as such it is not appropriate for this modeling approach. The CSC concrete model prediction exhibited less pinching than the experimental data and degradation of strength was higher. The CDP model prediction matched

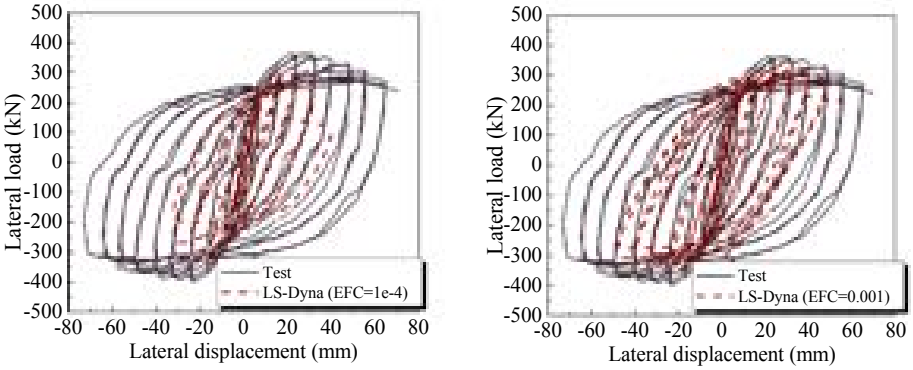

(a) ε_{fc}=0.0001 (default value)

(b) ε_{fc}=0.001

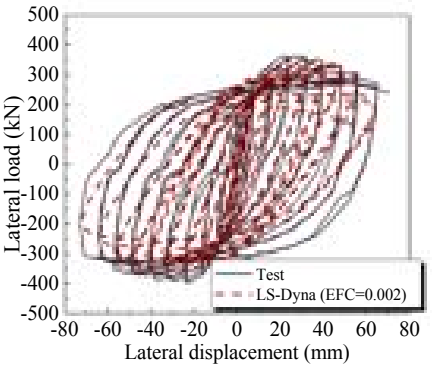

(c) ε_{fc}=0.002

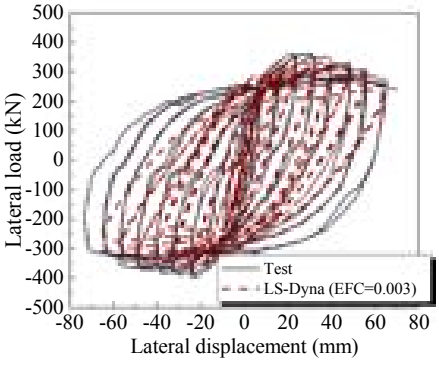

(d) ε_{fc}=0.003

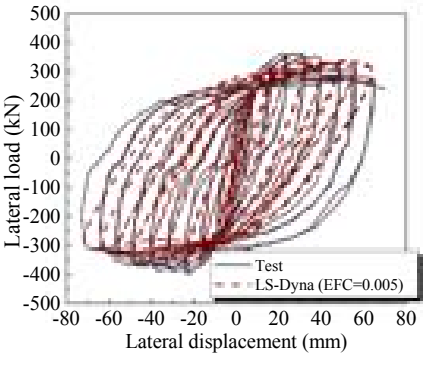

(e) ε_{fc}=0.005

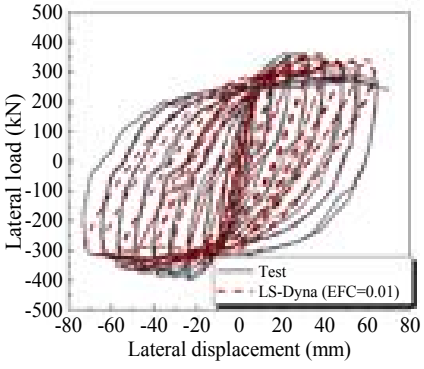

(f) ε_{fc}=0.01

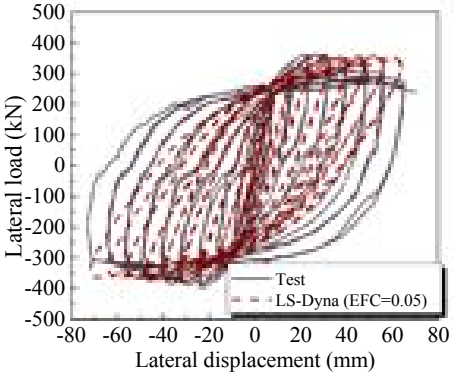

(g) ε_{fc}=0.05

Fig. 19. Predicted response with different damage parameters for the CDP model.

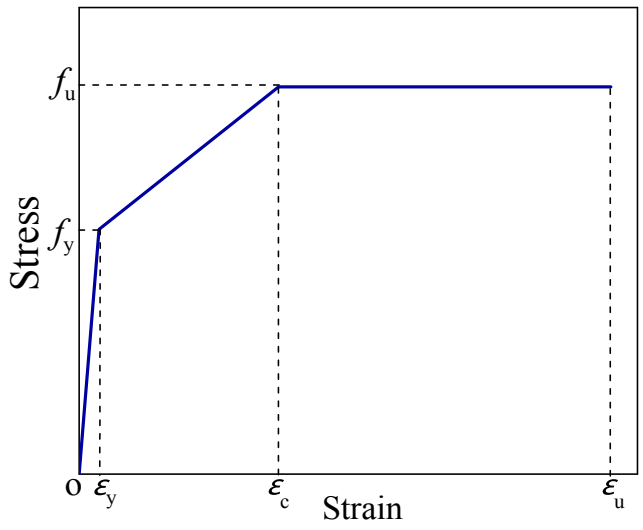

Fig. 20. Stress–strain relationship for steel tube.

the experimental data well, and the CDP model was used in the simulation of RC members. The accuracy of different concrete models was quantitatively evaluated in Table 1, in which the CDP model can provide the most accurate estimation of the resistance.

The default values for hardening and flow-rule parameters in the CDP model were used, and a bilinear damage model for concrete behavior in tension was selected. Fig. 9 shows the results of a study to determine the optimal damage parameter in compression, ε_{fc}, and the figure shows that the predicted results that the prediction with ε_{fc} between 0.0005 and 0.05 matched well with the experimental data, with the maximum difference of 0.9% of ultimate strength. Predicted results were not sensitive to the value of ε_{fc} within this range, and the damage parameter in compression was taken as 0.01 for confined concrete.

Considering different conditions of confinement in the concrete core and concrete cover, different values of ε_{fc} were used in the reinforcement-confined concrete core ($\varepsilon_{fc,core}$) and the concrete cover ($\varepsilon_{fc,cover}$). The concrete core confined by transverse reinforcement had the ε_{fc} value of 0.01 as determined above. Fig. 10 shows the simulation results with various $\varepsilon_{fc,cover}$ values. The figure shows that the prediction with $\varepsilon_{fc,cover}$ higher than 0.0001 can reasonably estimate the cyclic behavior of RC column. Predicted results were not sensitive to the value of $\varepsilon_{fc,cover}$ between 0.0005 and 0.01, and the damage factor for concrete

Table 3
Parameters of bond-slip model for different steel tube types for all concretes.

Tube type	*EN* (MPa)	*ET* (MPa)	*N* (MPa)	*T* (MPa)	*GIC*	*GIIC*
Straight-seam tube	6.5e−5	0.065	1e−5	0.032	0.01	0.44
Spiral-weld tube	2e−6	0.2	1e−5	0.75	0.01	1e6

cover was taken in the range as 0.005.

The reinforcement in RC columns was modeled with the Hughes-Liu beam element with four integration points and the "PLASTIC_KINEMATIC" steel constitutive model [43] shown in Fig. 11. The l_0 and l designate undeformed and deformed reinforcement lengths, E_p is the hardening stiffness of the bilinear stress–strain relationship, and β is the hardening parameter varying from zero to one (kinematic hardening if $\beta = 0$) and isotropic hardening if $\beta = 1$). Fig. 12 shows comparisons of computed and measured responses using different β values. The difference of the ultimate strength between the three β values was less than 4%, and the dissipated energy for the specimen with $\beta = 1$ was only 1.2% higher than that with $\beta = 0$. Therefore, the simulation results are not sensitive to β and thus the hardening parameter β was taken as 0.1.

The constant stress solid element results in hourglass shape when the element is subjected to bending [48]. The solid element with a reduced integration cannot detect strain when the element is in pure bending, leading to a zero-energy deformation mode in simulation results. An hourglass-like element shape can be observed in the bottom of the RC column in Fig. 13a and b. The Flanagan-Belytschko hourglass control [43] model was used to control this phenomenon. The hourglass coefficient was set as 0.03 to effectively inhibit hourglass modes, while minimizing the nonphysical stiffening of the cyclic response. The shape at the bottom of RC column using the Flanagan-Belytschko hourglass control is shown in Fig. 13c.

The bond-slip model proposed by Murcia-Delso et al. [26] was used to simulate response of the RC reinforcement embedded in concrete. In LS-Dyna, this model is established by using the constrained "BEAM_IN_SOLID" with defining the required function expressions. Fig. 14 illustrates the parameters of this model where τ_{max} is the bond strength, s_{peak} is the slip at the peak bond strength, and s_R is the clear rib spacing of reinforcement (usually a distance between 40% and 60% of the bar diameter). In absence of experimental data, τ_{max} and s_{peak} can be determined as:

$$\tau_{max} = 1.163 f_c^{3/4} \quad (23)$$

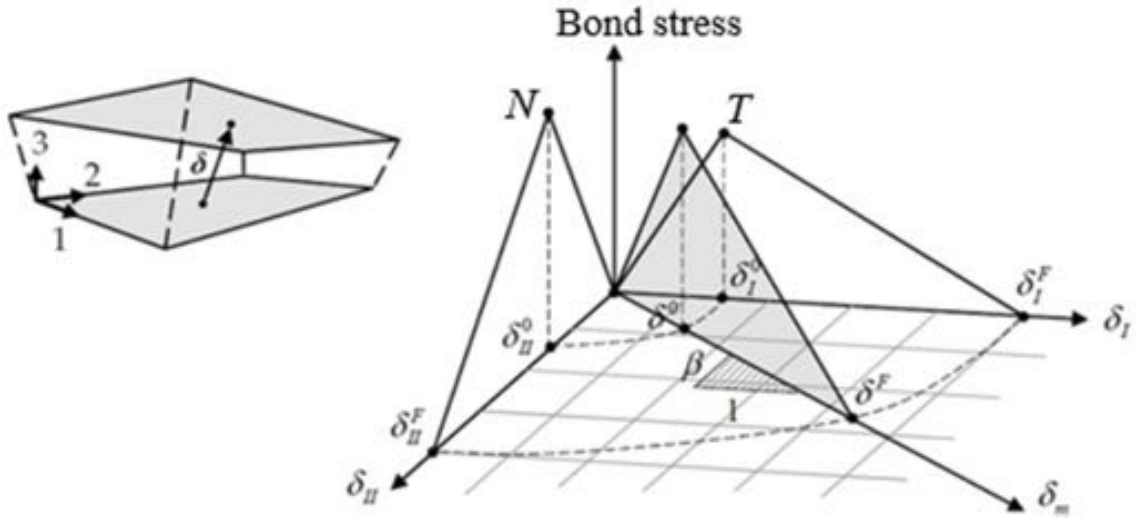

Fig. 21. Mixed-mode traction-slip law [43].

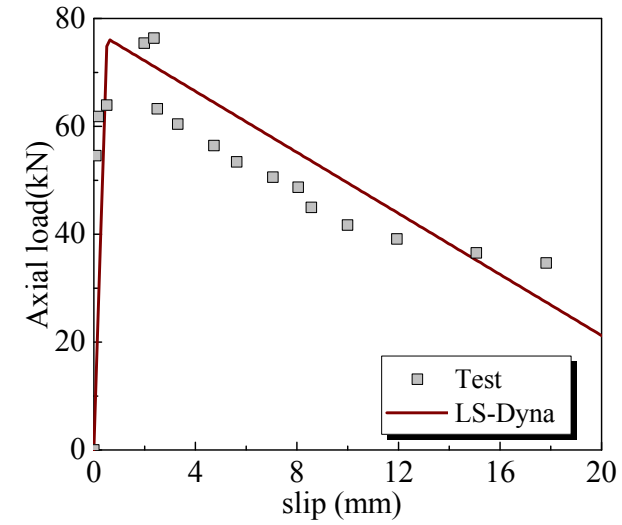

Fig. 22. Comparison of bond stress-slip response between predicted and test results.

$$s_{peak} = 0.07 d_b \quad (24)$$

where f'_c is the compressive strength of concrete and d_b is bar diameter.

3.3. Validation

The resulting model was further validated by comparison with experimental result from Specimen HC4-8L19-T10-0.2P [34], shown in Fig. 15. The model captured the load–displacement behavior of RC column with a maximum strength difference of 14.7%. Due to the accurate modeling of concrete and bond-slip of reinforcement, the shape of the predicted load–displacement curve is similar to the measured response, leading to similar energy dissipation between the predicted and measured results.

It is noted that the simulation results in Figs. 4, 8, 10, 12 and 15 are less accurate for the first load cycle. This has been found in prior research (e.g., [49]) investigating use of advanced nonlinear models. This is likely attributed to difference in the accuracy of the instrument used to measure the displacement. In most cases, and in the experimental research used in this study, a single instrument is used to monitor overall displacement. This instrument is calibrated for either the largest expected displacement or the full range of the instruments. This results in reduced accuracy of the horizontal transducers at small displacements. As a result, the predicted response appears to be less accurate but this is just as likely reduced accuracy in the test data.

4. Model development for concrete filled steel tubes

4.1. Experimental specimens for model Development: CFST tests [3–4]

Han et al. [4] investigated the seismic performance of hexagonal CFST columns encased in RC base as illustrated in Fig. 16. The height of RC base, axial load level, connection between the RC base and the CFST column, and the specimen size (scaled vs. full scale) were studied. The full-scale specimen with the lower height of RC case (CBL-2–0.3–2) was selected to evaluate modeling method. The hexagonal CFST had a sectional width (B) of 180 mm, tube thickness of 7.5 mm, effective length (L) of 1550 mm, outer component width (w_r) of 110 mm and outer component height of 600 mm. The cube compressive strength of RC base and concrete fill concrete (f_{cu}) were 52.3 MPa and 65.6 MPa, respectively. The yield strength for the steel tube was 262 MPa.

To determine the parameters for the tube to concrete bond model, the measured response of four bond CFST tests were used, as shown in Fig. 17 [3]. All specimens had circular tubes with outside diameter of 508 mm and wall thickness of 6.35 mm. The total height concrete fill was 1.524 m (the force was applied directly to the concrete fill and a 50 mm gap enabled this). There was a 25 mm gap between the base of the steel tube and concrete fill to permit relative movement of the concrete fill and steel tube. The steel tubes were either straight-seam or spiral-weld and the concrete fill was either conventional concrete or concrete with a low-shrinkage admixture. The straight-seam tube and spiral-weld tube without the low-shrinkage admixture were used to develop the modeling method. As shown in the figure, a universal testing machine was used to apply the vertical load to the concrete fill; external vibrating wire gages were used to determine the response of the steel tube, which, in turn, were used to determine the bond stress. As a basis of calibration, the test results were presented in Fig. 17b.

4.2. Analytical model

The CFST column to RC base connection was analyzed with the four different concrete models with comparisons between analyses and experiment shown in Fig. 18. Buckling of the steel tube as observed in the experiment [4] was predicted by the models using the CSC and CDP models, but was not predicted by the models using the other two concrete models. The CDP model had much better agreement with the experimental results than the CSC model, and so the CDP model was selected to simulate the behavior of CFST. The superior performance of CDP model can also be observed in the quantitative comparison in Table 2. The CDP model provided the best prediction of the resistance and reasonable estimation of dissipated energy (the energy prediction was nearer to the measured energy dissipation than K-C and Winfrith model).

A separate study was performed to determine the compressive damage parameter, ε_{fc}, for CFST. Fig. 19 shows the simulated vs. measured response for ε_{fc} values ranged from 0.0001 (default value) to 0.05 (all other modeling parameter kept constant). It can be seen lower ε_{fc} values of 0.0001 to 0.001 predicted sudden degradation not seen with the experimental data (see Fig. 19a and b). Models with ε_{fc} between 0.002 and 0.01 predicted the cyclic behavior with reasonable accuracy. An ε_{fc} value of 0.01 was adopted because its simulation results were closest to the measured response in both loading directions.

The steel tube was modeled using the Belytschko-Tsay shell element [50,51] with two integration points through the shell thickness with the PIECEWISE_LINEAR_PLASTICITY (MAT024) constitutive model with isotropic hardening [19]. This material type can define arbitrary stress

vs. strain curve and failure based on a plastic strain. In this context, a trilinear stress–strain relationship (see Fig. 20) is used to predict the behavior of steel tube. In the figure, the f_u and f_y represented ultimate strength and yield strength of steel tube. The ε_y, ε_c and ε_u donated the yielding strain, strain at the maximum stress and ultimate strain, respectively. Young's modulus of the steel (E_s) and Poisson's ratio were 207 GPa and 0.3, respectively, as established from a coupon test for research compared to the analysis [4]. The strain corresponding to the ultimate steel strength and failure strain were set as 0.1 and 0.25, respectively.

Unlike the RC column, the hourglass effect was not pronounced in CFST analysis. This was determined by comparing hourglass energy to the internal energy and was less than 2.8% of the internal energy.

Nonlinear springs between steel tube and concrete are a feasible method for modeling bond-slip behavior. However, this method was relatively expensive in calculation time and complicated for modeling. As a result, the fracture model for the cohesive material model "MAT_COHESIVE_MIXED_MODE" (MAT138 in LS-Dyna) was used to model bond-slip based on "AUTOMATIC_SURFACE_TO_SURFACE_TIEBREAK" contact in LS-Dyna with Option = 9. The details of this cohesive model are presented in Fig. 21.

In this figure, the δ_I and δ_{II} were the slips in the tangential and normal directions, respectively; δ_I^0 and δ_{II}^0 were the slips at the maximum bond stress; δ_I^F and δ_{II}^F were the ultimate slips in both directions; T and N represented the peak stress in tangential and normal direction, respectively. In this cohesive model, the ultimate slip was defined by:

$$\delta^F = \frac{2(1+\beta^2)}{\delta^0}\left[\left(\frac{EN}{GIC}\right)^{XMU} + \left(\frac{ET\times\beta^2}{GIIC}\right)^{XMU}\right]^{-\frac{1}{XMU}} \quad (25)$$

When XMU > 0. This equation can be expressed as B-K model when (XMU > 0):

$$\delta^F = \frac{2}{\delta^0\left(\frac{1}{1+\beta^2}EN^\gamma + \frac{\beta^2}{1+\beta^2}ET^\gamma\right)^{1/\gamma}}\left[GIC + (GIIC - GIC) + \left(\frac{ET\times\beta^2}{EN + ET\times\beta^2}\right)^{|XMU|}\right] \quad (26)$$

where EN and ET are the normal and tangential stiffness, respectively; GIC and $GIIC$ donate the energy releasing rate at normal and tangential directions; and β is the "mode mixity", which is defined as $\beta = \delta_{II}/\delta_I$.

The parameters in tangential direction in the contact model were calibrated using the results of the push-out test of CFST specimen (Fig. 17). The experiments by Stephens et al. [3] were used to determine ET, T and $GIIC$. In the normal direction, parameters of EN, N and GIC were set as approximately zero to simulate the initial slip condition between concrete core and steel tube [52,53]. The calibrated parameter values used in this paper are specified in Table 3. The comparison between the simulation results and experimental data was presented in Fig. 22. The LS-Dyna simulation predicted the experiment data well.

It should be noted that the bond strength in the tangential direction for the straight-seam tube was very low (0.032 MPa) [3]. This bond strength value would increase with the decreasing D/t of tube due to the

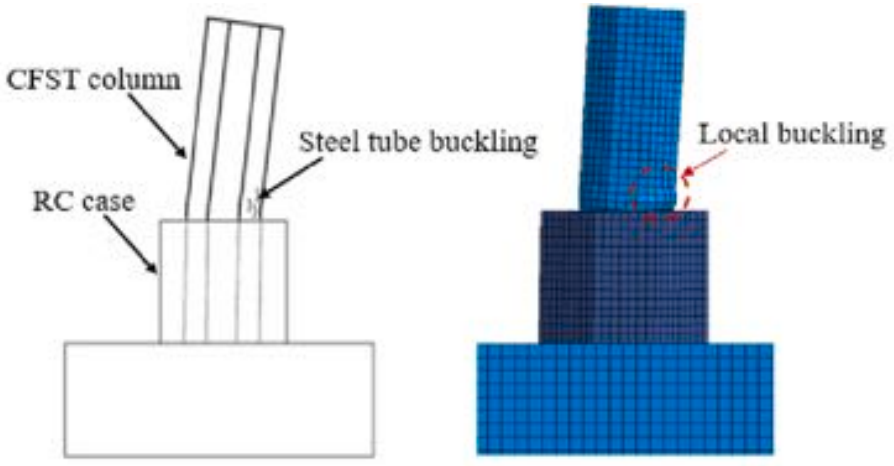

(a)Local buckling at drift ratio=6.7%

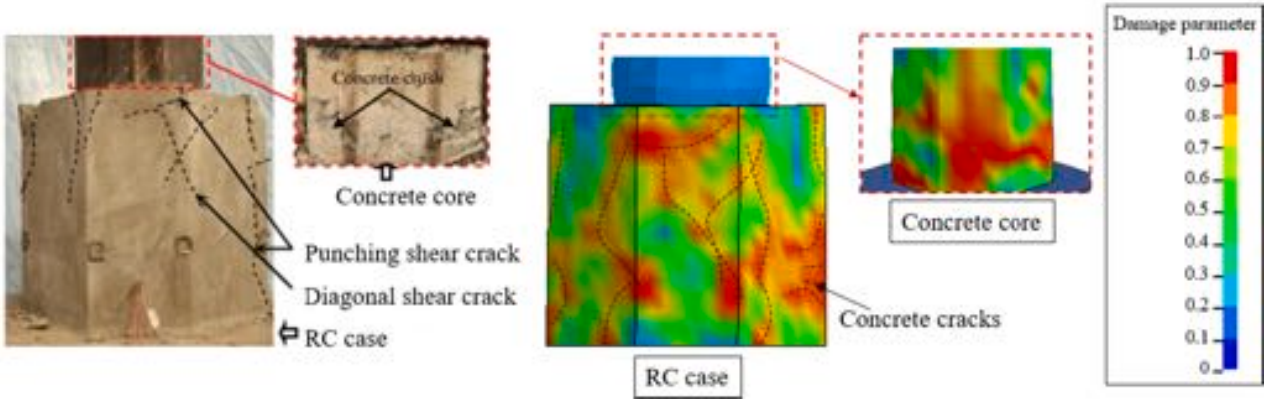

(a) Crack pattern

Fig. 23. Comparison of failure pattern between the predicted and test results from Han's experiment.

decreasing size of gap, which is induced by concrete shrinkage [24,54]. The linear relationship between bond strength and D/t proposed by Roeder et al. [54] can be used to predict CFST bond behavior with lower D/t (see Eq 27). It is reasonable to assume that the D/t ratio can significantly affect the bond behavior of CFST with spiral-weld tube, but the experimental evidence to support this assumption is not available. Thus, more experiments are still needed to be performed to investigate the influence of D/t ratio on the bond behavior of CFST using spiral-weld tube.

$$f_{\text{bond}} = 2.109 - 0.026(D/t) \text{ MPa} \quad (27)$$

4.3. Validation

Fig. 23 compares the predicted and observed steel tube buckling and cracking in the RC base [4]. The FE model provides reasonably accurate estimates of the observed behavior.

Figs. 24 and 25 compare the predicted and measured or observed experimental results from another study [35]. In this study, Specimen II was designed without adequate embedment; this specimen was selected because it sustained significant damage to the concrete footing and is challenging to model. Specimen III was selected because it has adequate embedment and a ductile response. These show the FE model predicts the load–displacement curves with the maximum strength difference of 0.5% and 4.3% for Specimens II and III, respectively. The cracking in the footing, concrete crushing and steel tube buckling are also accurately simulated in the model, and the predicted behavior accurately reflects differences in failure mode and performance.

It is of note that there are no standard methodologies for model validation. Clearly, there are additional tests that could be used. The test data used for the investigation and validation were selected because they represented typical section parameters, including reinforcement ratios and axial demands. The validation data were different than the original data used to investigate the model parameters and element types. Using a different set of data for investigation and validation is essential. In addition to comparing the measured force–displacement response, this paper also compares, in detail the damage patterns, cracks, bond-slip behavior between steel and concrete, etc. The comparisons in this paper is more comprehensive than most of other

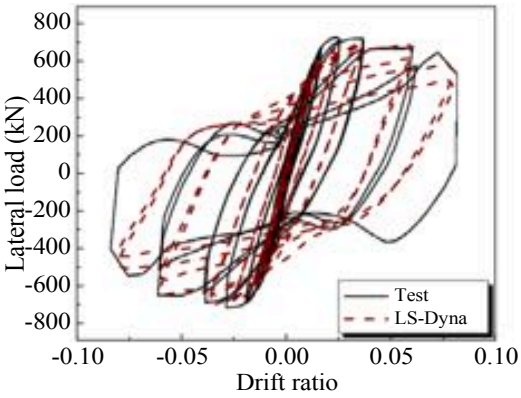

(a)Load-displacement curve

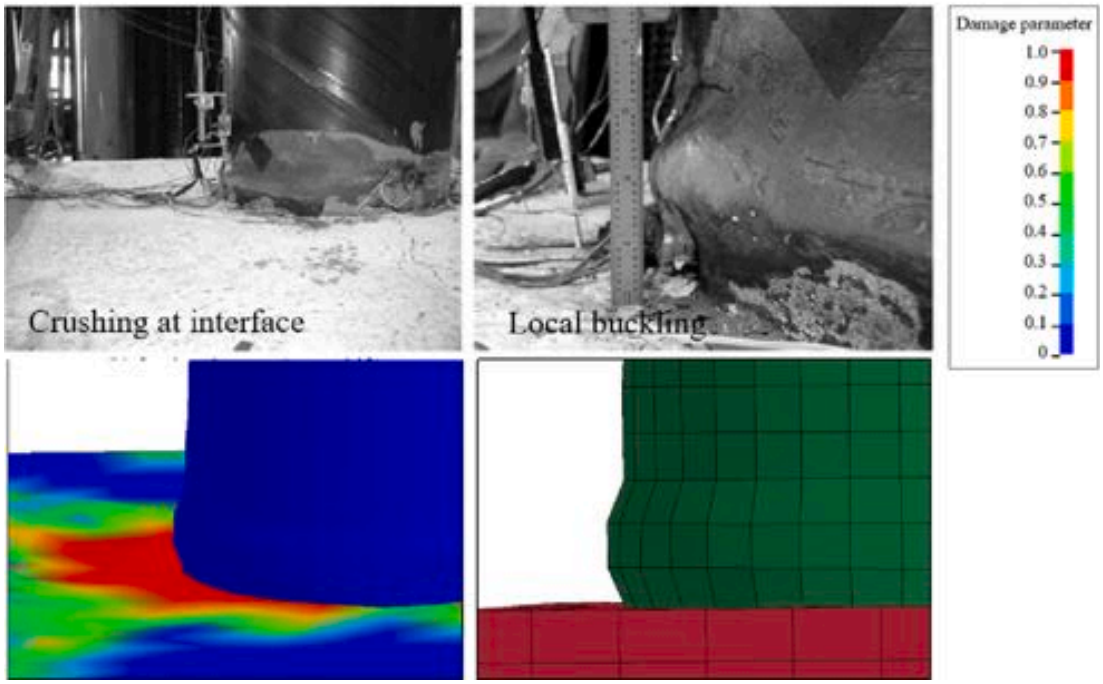

(b)Failure pattern

Fig. 24. Comparison between the predicted and test results from Roeder's experiment (Specimen III).

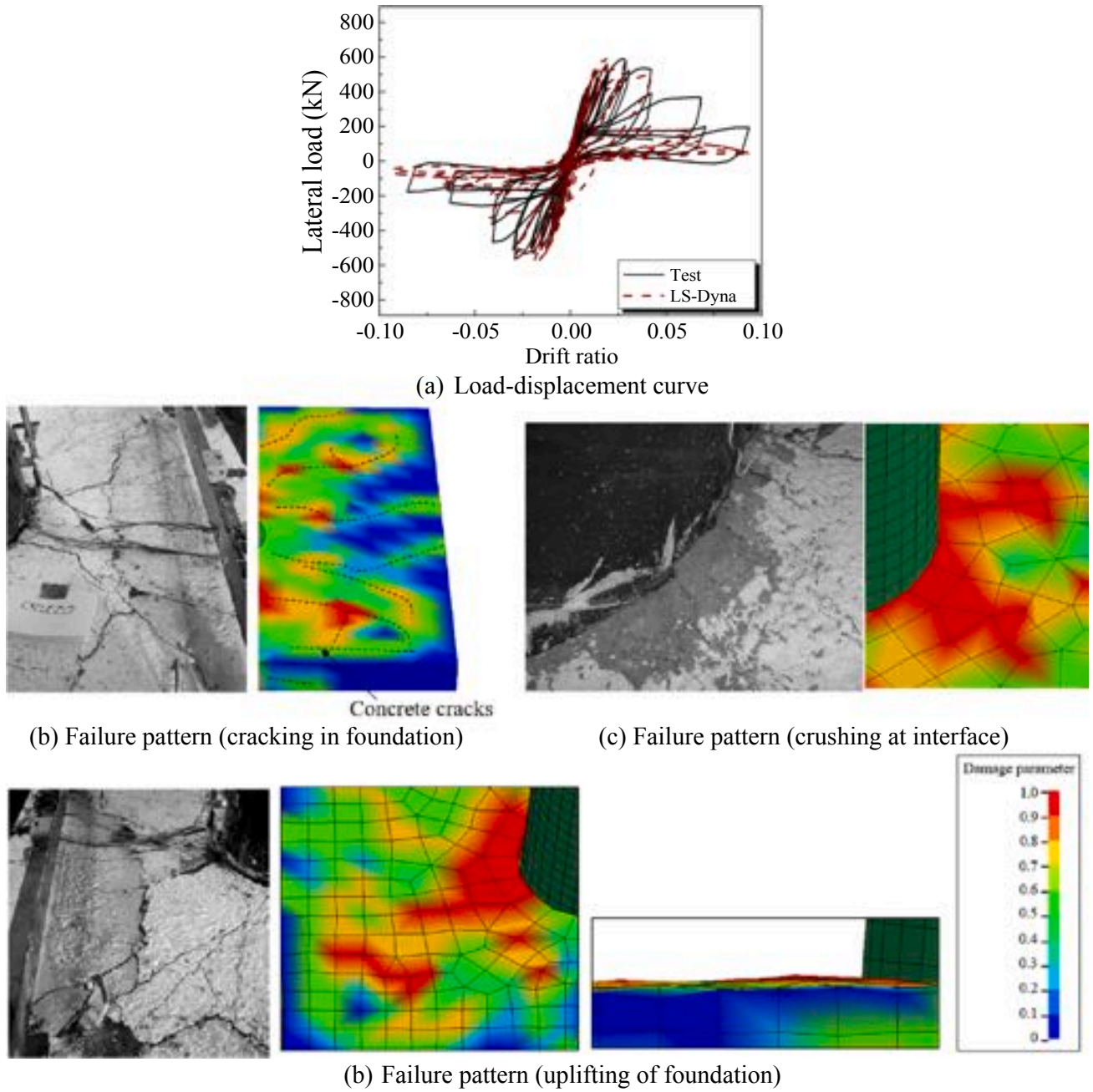

Fig. 25. Comparison between the predicted and test results from Roeder's experiment (Specimen II).

research [55–57]. Further validation will be required if the model is used to study different types of components, reinforcement detailing (such as lack of confining reinforcement), etc.

5. Summary of recommendations

This paper investigated and presented a general method to establish a FE model for RC and CFST specimen. For the ease of use and reference, all important recommendations are summarized in Table 4 as a guide for designers and researchers. The table includes the recommended constitutive models as well as the recommended values of all salient parameters in each component of the FE model.

6. Conclusions

This paper described nonlinear FE model recommendations in LS-Dyna for predicting the cyclic behavior of RC and CFST members and connections using the commercially available LS-Dyna nonlinear analysis software. Three groups of salient experimental results were selected to calibrate the important parameters in the model.

To select the most accurate concrete model, the predicted results with four commonly-used concrete models were compared against the measured responses for plain concrete, RC and CFST. The results showed that the prediction with concrete damage plasticity model (CDP model) agreed well with the test results. In the CDP model, the compressive damage factor (ε_{fc}) for confined concrete core was selected as 0.01 according to the comparative results, while the ε_{fc} value for concrete cover was taken as 0.005. The isotropic hardening model (MAT024) was used to simulate the constitutive behavior of steel tube. The combined hardening model (MAT003) was utilized for the reinforcement. The predicted results were not sensitive to the hardening parameter (β) in the model, and thus the β was selected as 0.1.

Table 4
Summary of modelling recommendations.

Components	Constitutive model	Parameters	Values
Concrete	CDP model	Compressive damage model	Exponential
		Tensile damage model	Bilinear
		Compressive damage parameter (ε_{fc})	0.005 (concrete cover) 0.01 (concrete core)
		Tensile damage parameter (w_f)	$4.444G_f/f_t$.
		Hardening parameters	Default values in LS-Dyna
Reinforcement	"PLASTIC_KINEMATIC" (MAT003 in LS-Dyna)	Combination parameter (β)	0.1
Steel tube	"PIECEWISE_LINEAR_PLASTICITY" (MAT024 in LS-Dyna)		
Bar-concrete interface	Bond-slip model proposed by Murcia-Delso et al. [26]		
Tube-concrete interface (straight-seam tube)	"MAT_COHESIVE_MIXED_MODE" (MAT138 in LS-Dyna)	Normal stiffness (*EN*)	6.5e-5
		Tangential stiffness (*ET*)	0.065
		Normal bond strength (*N*)	1e−5
		Tangential bond strength (*T*)	0.032 or Eq. (25)
		Normal energy releasing rate (*GIC*)	0.01
		Tangential energy releasing rate (*GIIC*)	0.44
Tube-concrete interface (spiral-weld tube)	"MAT_COHESIVE_MIXED_MODE" (MAT138 in LS-Dyna)	Normal stiffness (*EN*)	2e−6
		Tangential stiffness (*ET*)	0.2
		Normal bond strength (*N*)	1e−5
		Tangential bond strength(*T*)	0.75
		Normal energy releasing rate (*GIC*)	1e6

The FE model used constant stress solid element type (ELFORM = 1) to simulate the cyclic behavior of both RC and concrete fill in CFST. This choice resulted in the shortest calculation time and acceptable accuracy. The hourglass energy of the prediction in the concrete-encased CFST member was only 2.8% of the internal energy, indicating that hourglass effect can be ignored in the model. However, the hourglass-like element shape was observed in the analysis of RC members. Thus, Flanagan-Belytschko hourglass control was adopted in the simulation of RC columns, and the corresponding hourglass coefficient was set as 0.03.

The bond-slip behavior between the concrete fill and steel tube was reasonably modeled using the cohesive material model in LS-Dyna (MAT138). The key parameters in the tangential direction of the model were calibrated by comparison to test data. The bond stiffness, strength and energy releasing rate in the normal direction were set around zero to simulate the normally separation between concrete core and steel tube. In addition, the bond-slip behavior of reinforcement in RC member was modelled by the available bond-slip expression for bar-concrete interface.

Finally, the accuracy of the recommended FE model was evaluated. The modeling method in this paper predicted the load–displacement curves of RC and concrete-encased CFST columns with the maximum errors of 14.7% and 4.3% in resistance, respectively. In addition to the response, the FEM approach is capable of simulating general behavior and failure modes of both RC and CFST components. Additional validation is needed if the model is used to study different types of components, reinforcement detailing, etc.

Declaration of Competing Interest

None.

Acknowledgements

The research work in this paper is supported by the Short-term Visiting Program of Harbin Institute of Technology. The support received from Texas Advanced Computing Center (TACC) is also acknowledged.

References

[1] Stephens MT, Lehman DE, Roeder CW. Seismic performance modeling of concrete-filled steel tube bridges: Tools and case study. Eng Struct. 2018;165:88–105.
[2] Bruneau M, Kenarangi H, Murphy T P. Contribution of steel casing to single shaft fundation structural resistance. Report for National Cooperative Highway Research Program. Report Number 872;2018.
[3] Stephens MT, Berg LM, Lehman DE, Roeder CW. Seismic CFST column-to-precast cap beam connections for accelerated bridge construction. ASCE. J Struct Eng 2016.
[4] Xu W, Han LH, Li W. Seismic performance of concrete-encased column base for hexagonal concrete-filled steel tube: experimental study. J Constr Steel Res 2016;121:352–69.
[5] Dong YR, Xu ZD, Zeng K, Cheng Y, Xu C. Seismic behavior and cross-scale refinement model of damage evolution for RC shear walls. Eng Struct 2018;167:13–25.
[6] Demir A, Caglar N, Ozturk H, Sumer Y. Nonlinear finite element study on the improvement of shear capacity in reinforced concrete T-section beams by an alternative diagonal shear reinforcement. Eng Struct 2018;120:158–65.
[7] Ding FX, Yin GA, Jiang LZ, Bai Y. Composite fram of circular CFST column to steel-concrete composite beam under lateral cyclic loading. Thin-Wall Struct 2018;122:137–46.
[8] Han LH, Hou CC, Xu W. Seismic performance of concrete-encased column base for hexagonal concrete-filled steel tube: numerical study. J Constr Steel Res 2018;149:225–38.
[9] Lubliner J, Oliver J, Oller S, Oñate E. A Plastic-Damage Model for Concrete. Int J Solids Struct 1989;25:299–329.
[10] Lee J, Fenves GL. Plastic-damage model for cyclic loading of concrete structures. J Eng Mech 1998;124(8):892–900.
[11] Murcia-Delso J, Shing PB. Bond-slip model for detailed finite-element analysis of reinforced concrete structures. J Struct Eng 2015;141(4):04014125.
[12] Goto Y, Kumar GP, Kawanishi N. Nonlinear finite-element analysis for hysteretic behavior of thin-walled circular steel columns with in-filled concrete. J Struct Eng 2010;136(11):1413–22.
[13] Imani R. Post-Earthquake Fire Resistance of Ductile Concrete Filled Double-Skin Tube Columns. PhD thesis. Buffalo, NewYork: University at Buffalo; 2014.
[14] Grassl P, Jirasek M. Damage-plastic model for concrete failure. Int J Solids Struct 2006;43:7166–96.
[15] Grassl P, Xenos D, Uystrom U, Rempling R, Gylltoft K. CDPM2: A damage-plasticity approch to modeling the failure of concrete. Int J Solids Struct 2013;50:3805–16.
[16] Murray YD. User Manual for LS-DYNA Concrete Material Model 159; May 2007.
[17] Youssf O, ElGawady MA, Mills JE, Displaement and plastic hinge length of FRP-confined circular reinforced concrete columns, Eng Struct 2015;101:465–476.
[18] Moon JH, Lehman DE, Roeder CW, Lee HE. Evaluation of embeded concrete-filled tube (CFT) column-to-foundation connections. Eng Struct 2013;56:22–35.
[19] Moon J, Lehman DE, Roeder CW, Lee HE, Lee TH. Analytical evaluation of reinforced concrete pier and cast-in-steel-shell pile connecion behavior considering steel-concrete interface. Adv Mater Sci Eng 2016;2016:4159619.
[20] Wang JJ, Wang W, Qian XD. Progressive collapse simulation of the steel-concrete composite floor system considering ductile fracture of steel. Eng Struct 2019;200:109701.
[21] Cox JV, Herrmann LR. Development of a plasticity bond model for steel reinforcement. Mech Cohesive-Frict Mater 1996;3(2):155–80.
[22] Lundgren K. Pull-out tests of steel-encased specimens subjected to reversed cyclic loading. Mater Struct 2000;33(7):450–1196.
[23] Lundgren K, Gylltoft K, A model for the bond between concrete and reinforcement, Mag Concr Res;52(1):53–63.
[24] Eligehausen R, Popov EP, Bertero VV, Local bond stress–slip relationships of deformed bars under generalized excitations, UCB/EERC-83/23, Earthquake Engineering Research Center, 1983, University of California, Berkeley, CA.

[25] Lows LN, Moehle JP, Govindjee S, Concrete-steel bond model for used in finite element modeling of reinforced concrete structures. ACI Struct J;101(4):501–511.
[26] Murcia-Delso J, Stavridis A, Shing B. Modeling the bond-slip behavior of confined large-diameter reinforcing bars. III ECCOMAS Thematic Conference on Computational Methods in Structural Dynamics and Earthquake Engineering, Corfu, Greece; 2011. p. 25–28.
[27] Tao Z, Song TY, Uy B, Han LH. Bond behavior in concrete-filled steel tubes. J Constr Steel Res 2016;120:81–93.
[28] Lyu WQ, Han LH. Investigation on bond strength between recycled aggregate concrete (RAC) and steel tube in RAC-filled steel tubes. J Constr Steel Res 2019; 155:438–59.
[29] Guan MS, Lai ZC, Xiao Q, Du HB, Zhang K. Bond behavior of concrete-filled steel tube columns using manufactured sand (MS-CFT). Eng Struct 2019;187:199–208.
[30] Baltay P, Gjelsvik A. Coefficient of friction for steel on concrete at high normal stress. J Mater Civ Eng 1990;2(1):46–9.
[31] Han LH, Wang WD, Zhao XL. Behavior of steel beam to concrete-filled SHS column frames: Finite element model and verification. Eng Struct 2008;30:1647–58.
[32] Peng Z, Dai SB, Pi YL, Li DX, Zhang YC, Huang J. Seismic behavior of innovative ring-bar reinforced connections composed of T-shaped CFST columns and RC beams with slabs. Thin-Wall Struct 2018;127:1–16.
[33] Low SS, Moehle JP. Experimental study of reinforced concrete columns subjected to multi-axial cyclic loading, EERC Report 87/14. Earthquake Engineering Research Center: University of California, Berkeley, USA; 1987.
[34] Xiao Y, Martirossyan A. Seismic performance of high-strength concrete columns. J Struct Eng 1998;124(3):241–51.
[35] Lehman DE, Roeder CW. Foundation connections for circular concrete-filled tubes. J Constr Steel Res. 2012;78:212–25.
[36] Liu B, Fan W, Guo W, Chen BS, Liu R. Experimental investigation and improved FE modeling of axially-loaded circular RC columns under lateral impact loading. Eng Struct 2017;152:619–42.
[37] Epackachi S, Whittaker AS. A validated numerical model for predicting the in-plane seismic response of lightly reinforced, low-aspected ratio reinforced concrete shear walls. Eng Struct 2018;168:589–611.
[38] Sinha BP, Gerstle KH, Tulin LG. Stress-strain relations for concrete under cyclic loading. ACI J 1964;61(2):195–212.
[39] Gopalaratnam VS, Shah SP. Softening response of plain concrete in direct tension. ACI J 1985;82(3):310–23.
[40] Wang Junjie. Personal Communication; 2020.
[41] Malvar LJ, Crawford JE, Wesevich JW, Simons D. A plasticity concrete material model for DYNA3D. Int J Impact Engng 1997;19:847–73.
[42] Chen WF. Plasticity in Reinforced Concrete. New York: McGraw Hill; 1982.
[43] LSTC. Keyword User's Manual, Volume II. Livermore, CA, USA: Version 11 R11.0.0; 2019.
[44] Broadhouse BJ, Neilson A. Modeling reinforced concrete structures in DYNA3D, Report:DYNA3D user group conference. London 1987.
[45] Ottosen NS. A failure criterion for concrete. J Eng Mech Divis 1977;103:527–35.
[46] International Federation for Structural Concrete (fib). CEB-FIP model code 2010 (MC2010). Berlin, Germany: Ernst & Sohn; 2013.
[47] Rubin M. A simple, convenient isotropic failure surface. ASCE J Eng Mech 1991; 117:348–69.
[48] Belytschko T, Ong JSJ, Liu WK, Kennedy JM. Hourglass control in linear and nonlinear problems. Comput Methods Appl Mech Eng 1984;43(3):251–76.
[49] Pugh JS, Lowes LN, Lehman DE. Nonlinear line-element modeling of flexural reinforced concrete walls. Eng Struct 2015;104:174–92.
[50] LSTC. Keyword User's Manual, Volume I. Livermore, CA, USA: Version 11 R11.0.0; 2019.
[51] LSTC. Theory Manual. Livermore, CA, USA: r10859; 2019.
[52] Nguyen DH, Hong WK, Ko HJ, Kim SK. Finite element model for the interface between steel and concrete of CFST (concrete-filled steel tube). Eng Struct 2019; 185:141–58.
[53] Zhang YB, Han LH. Zhou Kan, Yang ST, Mechanical performance of hexagonal multi-cell concrete-filled steel tubular (CFST) stub columns under axial compression. Thin-Wall Struct 2019;134:71–83.
[54] Roeder CW, Cameron B, Brown CB. Composite action in concrete filled tubes. J Struct Eng 1999;125(5):477–84.
[55] Han LH, Wang WD, Tao Z. Performance of circular CFST column to steel beam frames under lateral cyclic loading. J Constr Steel Res 2011;67:876–90.
[56] Zhu HQ, Li Y, Zhang XD. Rigidity estimation of embedded CFST column-to-beam connections. Eng Struct 2017;147:768–81.
[57] Wang K, Lu XF, Yuan SF, Cao DF, Chen ZX. Analysis on hysteretic behavior of composite frames with concrete-encased CFST columns. J Constr Steel Res 2017; 135:176–86.